# Development, Preparation, and Characterization of High-Performance Superconducting Materials for Space Applications

A Progress Report submitted to NASA
For Grant: NAG 5 1017

by

Dr. Arthur N. Thorpe
Physics Department
Howard University
Washington, D.C. 20059

in conjunction with

Dr. Aaron Barkatt
Department of Chemistry
The Catholic University of America
Washington, D.C. 20064

December 1991

A summary of the work which has been completed on this project during the past reporting period is included and a paper which has been prepared for publication. This paper is being submitted as a progress report for grant number NAG 5 1017 for this period.

# MELT-PROCESSED YBCO SUPERCONDUCTORS: PROCESSING AND PROPERTIES

H. Hojaji*, S. Hu*, A. Barkatt*,
A. N. Thorpe**, and D.D. Davis**

* The Catholic University of America, Washington, DC
** Howard University, Washington, DC

## ABSTRACT

The preparation of high-temperature superconducting ceramics in bulk form is a major challenge in materials science. For practical applications, such bulk materials must have high magnetization, high critical current capabilities, and a high degree of stability of these properties as a function of time at operational temperatures up to around 77 K. These properties require, on one hand, elimination of weak links from the structure and, on the other, introduction of sufficiently high concentrations of defect centers to produce effective pinning of the flux matrix. The most promising route to the production of high-quality bulk specimens involves melt processing of Y-Ba-Cu-O materials.

The current status of both partial melting and melt quenching techniques, with or without an intermediate powder processing stage, are described in detail, and the

problems associated with each of the methods are discussed. Results of studies performed on melt-processed materials prepared at the authors' laboratory and elsewhere are reported and discussed, with an emphasis on magnetization and on other physical properties associated with it, such as critical current density, levitation force, and flux creep. The nature of structural features which give rise to flux pinning, including both small and large defects, is discussed with reference to theoretical considerations. The rates of flux creep and the factors involved in attempting to retard the decay of the magnetization are surveyed. Finally, recently discovered magnetization anomalies, involving an increase in magnetization with increasing applied magnetic field over a certain range of field intensities, are described and their origin ascribed to the removal of proximity coupling or Josephson coupling of certain defects at higher fields.

# I - INTRODUCTION

Since the discovery of high temperature superconducting oxide La-Sr-Cu-O with a critical temperature ($T_c$) of 35 K in 1986 [1], great progress has been made in this area. In early 1987, the discovery of a Y-Ba-Cu-O compound [2] with a $T_c$ of 92 K gave a great boost to the field of high temperature superconductivity, since it made it possible to use liquid nitrogen refrigeration, which is much simpler and more accessible than the use of liquid helium. In early 1988, a bismuth-based compound, Bi-Sr-Ca-Cu-O, with a $T_c$ of 110 K was discovered[3]. Soon after, the discovery of a Tl-Sr-Ca-Cu-O compound with a still higher $T_c$ of 125 K was made[4]. Our current understanding of these new materials has grown rapidly during the past five years, due to the enormous amount of research that has been performed on these materials worldwide. Compounds based on $Y_1Ba_2Cu_3O_{7-x}$ (so called 123) are the most heavily studied of these new copper oxide-based superconductors. Much of the progress has been through the use of single crystals, which has provided insight into the structure, magnetization, flux pinning and creep mechanisms, etc. It is clear that most of the practical applications of HTC superconductors are contingent upon achieving high critical current. The upper value of the critical current density, based on the calculated value from Ginzburg-Landau equation [5], is 2.3 x $10^8$ A/cm$^2$ at 0 K, which decreases to 2.7 x $10^7$ A/cm$^2$ at 77 K, in an applied field of 1 tesla. Remarkably, in epitaxial thin films of YBCO deposited on a $SrTiO_3$

substrate, $J_c$ values above $10^6$ A/cm$^2$ at 1 tesla applied field have been reported[6]. However, in virgin single crystals of YBCO, only values around 1000 A/cm$^2$ at 1 tesla and 77 K have been obtained[7]. Furthermore, in poly- crystalline 123 materials, made by regular solid state sintering, the grains are weakly coupled together, lowering the bulk $J_c$ value to about 100 A/cm$^2$ at zero applied field.

It is known that HTC superconductors have an anisotropic crystal structure which results in strongly anisotropic electrical and magnetic properties. This crystalline anisotropy manifests itself more dramatically in terms of limiting current densities in the bulk polycrystalline materials than in thin films, since thin films are grown epitaxially on the substrates. Consequently, crystal alignment is also necessary for bulk materials, in order to achieve high critical current densities.

In the past four years, great progress has been made in eliminating intergranular and high angle boundaries in polycrystalline superconductors by using so-called ***melt processing techniques***. Among these techniques are, melt texturing[8], partial melt growth [9, 10], and various melt quenching techniques [11, 12, 13, 14]. These techniques have been used to produce bulk samples with current densities exceeding 3 x $10^4$ A/cm$^2$ at 77 K and 1 tesla.

In spite of major improvements in $J_c$, large relaxation effects causing a decay of the magnetization and of the persistent current have been observed. This effect is called ***flux creep***. It is a thermally activated process which is mainly due to a combination of low pinning potentials and of relatively high temperatures (i.e. 77 K) at which these materials are intended to be used. Stated in simple terms, jumping of trapped-flux lines

from one pinning region to another causes the creep. In various HTC superconductors, flux creep has been a major challenge for researchers since coherence lengths are extremely small, having values in the order of 10 A, and as a result, flux vortex migration can readily take place. In principle, the creep rate can be decreased by increasing the pinning potential. Even though the origin of the pinning in HTC superconductors is still the subject of considerable discussion, the main pinning mechanisms are being recognized as intrinsic pinning [15], pinning by extended defects such as intergrowths and boundaries [16], pinning by second phase inclusions [17, 18], or by point or columnar defects [19, 20]. Neutron irradiated YBCO single crystals have produced $J_c$ values in the order of $6 \times 10^5$ A/cm$^2$, an improvement of almost two orders of magnitude over un-irradiated crystals. This remarkable improvement is believed to be caused by inducing point defects with sizes of the order of the coherence length. In thin films of YBCO, the natural existence of numerous screw dislocations and columnar holes is believed to be responsible for providing effective pinning sites [21].

The achievement of high $J_c$ in single crystals indicates that it is possible to increase the $J_c$ values in bulk polycrystalline YBCO superconductors by eliminating all the weak links and cracks and aligning the crystals. In other words, processing techniques should be optimized to produce the necessary concentration of flux pinning centers while eliminating weak link features.

The use of HTC materials for large scale applications requiring high $J_c$ values will become possible only upon utilizing high quality bulk materials, rather than millimeter size single crystals, since irradiation methods are less than ideal as a basis for the

manufacturing process. Therefore the development of processing methods to produce large pieces of polycrystalline bulk HTC materials with appropriate pinning sites is very important.

In the following chapters, various melt processing techniques capable of producing high-quality bulk specimens of superconducting YBCO will be discussed. The magnetization characteristics of these materials, which include magnetic hysteresis loops and creep data will be correlated with the corresponding microstructure and with possible pinning mechanisms.

## II - THE PHASE DIAGRAM OF YBCO

The equilibrium phase diagram of YBCO is a complex one. Various pseudo-binary and ternary equilibrium phase diagrams have been proposed [22, 23, 24], but to date no consensus has been reached as to the exact locations of various phase boundaries. This is due mostly to the critical rule of oxygen in all the phase compositions and phase equilibria in the system. The processing temperatures used in conventional solid state sintering of YBCO are normally below the lowest peritectic reaction temperature in the system and thus the phase considerations are relatively straightforward. The only major processes which appear to be involved around the stoichiometric 123 composition are the reactions between the Y, Ba and Cu precursors to form the ternary compound and the oxygen-controlled interconversion of the insulating tetragonal phase and the

superconducting orthorhombic phase. However, in the melt processing techniques, the processing temperatures exceed one or several eutectic and peritectic temperatures, which makes the processing considerably more complicated than regular solid state sintering. Furthermore, additional superconducting compounds in the YBCO system, such as the 124 compound with a $T_2$ of about 85 K, can be synthesized under high oxygen pressure [25]. Therefore, the complexity of the relevant phase diagrams increases due to added P-T surfaces.

In this review paper, we limit our discussion to the region around the 123 composition since there is far more information available on this system than on any of the other HTC superconducting systems.

One of the recent phase diagrams of YBCO, adapted from K. Dembinski et al. [26], is illustrated in Figure 1. The various eutectic and peritectic reactions and temperatures are given below.

$e_1$ 915 $123 + BaCuO_2 + CuO \text{ ----> } L$

$e_2$ 920 $BaCuO_2 + CuO \text{ ----> } L$

$P_1$ 940 $123 + CuO \text{ ----> } 211 + L$

$P_2$ 975 $211 + CuO \text{ ----> } Y_2Cu_2O_5 + L$

$P_3$ 1000 $BaCuO_2 + 123 \text{ ----> } 211 + L$

$P_4$ 1010 $123 \text{ ----> } 211 + L$

$e_4$ 1100 $Y_2Cu_2O_5 + CuO \text{ ----> } L$

$P_5$ 1125 $Y_2Cu_2O_5 \text{ ----> } Y_2O_3 + L$

$P_6$ 1270 211 ----> $Y_2O_3$ + L

Of prime interest in the melt processing techniques is the vertical cut through the phase diagram at the stoichiometric 123 composition. As illustrated in Figure 1, the 123 solid phase decomposes sequentially into 211 and $Y_2O_3$ solid phases before complete melting. Each one of the melt processing techniques described below is associated with a specific sequence of decomposition and re-formation reactions of various solid phases, followed by phase growth in the region of stability of a particular phase.

## III - MELT PROCESSING

The stimulus for the development of melt processing techniques has been the demand for high-quality HTC materials, i.e. materials combining high current density ($J_c$) and large magnetization with high mechanical strength. In recent years it was realized that the attainment of high $J_c$ and strong magnetization (e.g. for levitation purposes) requires materials in which weak links, involving features such as cracks, voids, high-angle grain boundaries, and insulating phases at grain boundaries, are eliminated. At the same time, a sufficiently high concentration of flux pinning sites (certain defects, impurities or second phases) has to be present. Conventional solid state sintering, which was extensively employed during the early development of HTC materials, yields materials with low $J_c$ values due to the presence of an excessive number of weak links.

These materials also tend to have low density and poor mechanical strength. On the other hand, large, pure and stress-free single crystals of 123 cannot be expected to contain enough flux pinning centers. Accordingly, the most promising materials for HTC applications are polycrystalline materials made by melt-based techniques, since such materials can provide, on one hand, high density and a high degree of grain alignment to minimize the number of weak links, and on the other hand, a sufficient number of defects to serve as flux pinning centers. As described below, melt-based techniques can be controlled to produce second phases such as 211 ($Y_2BaCuO_5$), which provide effective flux pinning sites.

There are many different types of melt processing techniques which are described in the literature. These techniques can be divided, in general, into two major categories, viz. partial melting and melt quenching. Melt processing techniques are complex because of the many processing parameters involved. The development of optimized techniques has been the subject of extensive work at the authors' laboratory and by other groups. For each technique, partial melting and melt quenching, two variations will be described. One of them involves thermal treatments on the bulk YBCO specimen as a whole, and the other includes a stage during which the material produced by initial melt-based treatments is ground into powder and the powder used in the stages leading to the final product. Figure 2 illustrates the flow diagrams of these four processing methods.

1. Partial Melting

Partial melting or partial melt growth was initially designed to take advantage of

liquid phase sintering [9]. While there are many variations of this technique, the principal steps are to form the liquid phase by heating a pre-calcined $YBa_2Cu_3O_{7-x}$ material to a temperature above that of the first peritectic reaction as shown earlier. The highest temperature is usually between 1010-1150°C, depending on the composition and method employed, resulting in the formation of a Cu-rich liquid phase and a 211 solid phase. The needle-like 211 crystals are relatively coarse, having an average size of 10-100 microns depending on the highest temperature employed. The heat treatment is followed by slow cooling (e.g. 1-10°C/hr) from a temperature of 0-50°C above that of the peritectic reaction to below 950°C. During this step the 123 phase is nucleated and plate-like grains, which grow in the ab planes, are formed to produce a layered structure. The size and thickness of these plates depend on the initial composition, the oxygen partial pressure and the cooling rate. Slow cooling is further continued in an oxygen environment to below 300°C, transforming the insulating 123 tetragonal phase to the superconducting orthorhombic phase. Jin et al. [8] used a procedure similar to the one described above but applied a temperature gradient during the nucleation and growth stage. The so called texturing process has been commonly used for metallic alloys and it is believed to produce uni-directional solidification. 123 samples made by the texturing process exhibited critical current densities as high as $1.7 \times 10^4$ A/cm$^2$ at zero applied field, and $4 \times 10^3$ A/cm$^2$ at 1 tesla, all at 77 K. The natural tendency of the system to grow a layered crystalline structure was demonstrated by Salama et al. [10], who used a very slow cooling rate of 1°C/min from 1030°C to 980°C. Using this method they obtained samples which exhibited transport current densities of $1.8 \times 10^4$ A/cm$^2$ at zero

field and 77 K. Hu [12] used a similar slow cooling process but increased the oxygen pressure to several atmospheres during the cooling stage. He obtained samples that had current densities as high as 2.1 x $10^4$ A/cm$^2$ at zero applied field, and 1.3 X $10^4$ A/cm$^2$ at 0.8 tesla, all at 77 K.

The partial melting techniques, however, appear to have a relatively severe shortcoming. Incongruent melting of YBCO above the first peritectic reaction produces a liquid phase which tends to diffuse out to the exterior as a result of surface tension and low viscosity. In the case of larger samples, vertical drainage is very likely to take place. The depletion of the liquid phase from the interior of the specimens hinders the grain growth and texturing processes during the cool-down stage from above the peritectic reaction temperature. The problem is much more severe for specimens with large cross sections in a uniform temperature zone. Bars and cylinders 5 cm long with small cross sections, usually less than 5 mm, have been partially melted by pushing them into a hot zone at a linear speed of several mm/hr and a temperature gradient of 50°C/cm [27]. Clearly, this procedure can be used to produce high-quality thin rods, but unfortunately it is not suitable for fabrication of articles with a large cross sectional area.

2. Mixed-Powder-Partial-Melting (MPPM)

In the MPPM process, 211 phase pure powder is mixed with a Y-Ba-Cu-O pre-calcined powder. The yttrium content of the YBCO precursor can vary from the stoichiometric 123 ratio [28] to about zero [29]. The resulting mixture is then heated to above the first peritectic reaction temperature, and is slowly cooled through the peritectic

range to react the 211 phase with the liquid phase present to form 123 with residual 211 providing pinning centers. We have also studied this method extensively with varying target concentrations of yttrium in the final product. Again, this method, like all other partial melting techniques, suffers from extensive loss of the liquid phase at high temperatures when fabricating large specimens.

The main advantage of various partial melting techniques is that they do not require complete melting, which is normally done in a crucible. Molten YBCO is very reactive and dissolves almost any crucible materials with which it comes in contact, even noble metals such as platinum and rhodium. Accordingly, the use of partial melting procedures, with the liquid largely confined within the solid structure of the YBCO material, minimizes the problem of attack by the reactive melt on the crucible and the resulting contamination of the melt by dissolved crucible material.

3. Melt Quench Processing

It has been well established that the presence of fine and uniformly distributed 211 particles in the liquid phase at the onset of the first peritectic reaction is a key factor in the development of a well aligned structure with a minimum number of weak links. The resulting microstructure of such a system consists of a multitude of aligned platelets with a very fine 211 distribution, which is believed to play an important role in flux pinning. Partial melting alone cannot produce a well distributed 211 phase in large samples, because prolonged heating above the peritectic reaction temperature results in the liquid phase segregation and drainage as discussed above. Consequently, it was found that if

the heating is carried out above the second peritectic reaction temperature, 211 decomposes into $Y_2O_3$ and a Ba-Cu-O rich liquid phase. At this stage, the mixture has a low viscosity and can be quenched to freeze the high-temperature structure. Subsequent heating above the first peritectic reaction temperature results in the nucleation and growth of the 211 phase at the $Y_2O_3$ sites, and thus a uniform distribution of 211 is obtained. The annealing process is continued by rapid cooling to about 1000-1050°C, and follows similar cooling schedules to those described for the partial melting process.

There are several variations of this method but in all cases a precursor of YBCO is melted at high temperature, normally above 1350°C. Different groups have used different terminologies and abbreviations for their processes, several of which are listed below:

| | | |
|---|---|---|
| QMG | Quench and Melt-Growth | Ref [17] |
| MPMG | Melt-Powder-Melt-Growth | Ref [30] |
| MQ | Melt-Quenched | Ref [14] |
| MQPPMG | Melt-Quenched-Pressurized-Partial-Melt-Growth | Ref[31] |

The YBCO precursor is normally calcined several times before melting. However, pre-calcined mixtures of $Y_2O_3$, CuO, and $BaCO_3$ have also been used. The composition is centered around 123, but small deviations are also common, especially with slight enrichment with respect to yttrium or with additions of other oxides to increase the number of pinning centers. For more details see Ref [14], which describes studies

involving compositions with excess yttrium or with added Gd, Tb, Ho, Yb, or Nb. There are not many materials which can be used for melting containers, because of the extreme corrosivity of molten YBCO materials at temperatures above 1400°C. Platinum crucibles seem to be the best choice at the present time, despite their being dissolved away at a level of 0.2-1.5 wt% in the melt at about 1450°C. For melting of short duration, about 10 minutes at 1450°C, the level of Pt in the melt is about 0.5%. Not much information is available about the effect of the presence of platinum on the YBCO system. It is believed that platinum forms a compound with Ba and Cu oxides which has a crystalline structure similar to that of 123 [32, 33]. This phase is finely dispersed in the final 123 matrix and may in fact play an important role in flux pinning. More studies are presently under way to determine the effects of the presence of platinum in YBCO superconductors.

There have been reports of two methods of containerless melting in the literature. The first method [34] consists of heating small particles of 123 material very quickly above 1450°C in an inductively heated vertical tube furnace. The temperature of the hot zone of the furnace can reach 1600°C. At the receiving end of the furnace, the molten droplets are quenched very rapidly on a chilled copper wheel. The resulting product is a finely dispersed $Y_2O_3$ phase 1-2 micron across in a matrix of Ba-Cu-O phase.

According to the second method [35], sintered 123 pellets are melted with an $H_2$-$O_2$ torch ($O_2$ rich flame), and the droplets are rapidly quenched in a high speed twin rolling mill to form thin flakes. The key to the success of the melt quenching technique is to obtain very fine dispersion of $Y_2O_3$ in a Ba-Cu-O rich liquid phase. Since $Y_2O_3$

agglomerates very quickly at high temperature, it is necessary to shorten the melting time as much as possible. As a result, crucible melting may not be suitable for producing large quantities of melt quenched materials, and other continuous methods with a short residence time of the melt in the furnace are required.

4. Melt-Powder-Melt-Growth

Several problems are encountered with the melt quench and partial melting technique when sample size becomes large, i.e. more than 10 mm in diameter. First, reheating the specimen above the first peritectic reaction temperature to the region where the 211 phase is stable produces a large volume fraction of liquid relative to the amount of the solid 211 phase. The reaction is very fast, and if it is not controlled properly, it results in formation of large grains of 211, defeating the purpose of the melt quenching process. In addition, due to its low viscosity, the liquid phase in contact with 211 can drain out easily, as described in the section on partial melting, and leave behind a large amount of porosity in the final product. To alleviate these problems and yet benefit from the melt quenching technique, two methods have been proposed. In the first method [30], the melt quenched specimens are ground and pressed into different shapes before partial melting. This additional step produces a more homogenous distribution of $Y_2O_3$, and consequently finer dispersion of residual 211 phase in the final superconducting 123 material. The second method [31] is to apply an external pressure at elevated temperatures. It is observed that the bulk YBCO materials have high plasticity above the first peritectic reaction temperature, and this is accompanied by the formation of a

relatively dense skin at their outer surfaces. The external pressure squeezes the outer skin and prevents the liquid from draining. As a result, larger specimens have been fabricated without serious loss of the liquid phase, and these specimens have dense 123 superconducting structures.

## IV - PHYSICAL PROPERTY MEASUREMENTS

### 1. Transport Critical Current

It is customary to determine the current density by passing a dc current through the sample and measuring the voltage by the

standard four point technique. The four-point technique of measuring resistance is based on having two leads or probes carry a known constant current I into and out of the specimen, while the other two leads are used to measure the potential drop between two equipotential surfaces resulting from the current flow. For superconducting specimens the leads are often arranged in a linear configuration, with the contacts for the input current on the ends, and those for the measurement voltage near the center. The method is very suitable for thin films and wires, but it generates catastrophic warm-up in the cases of bulk samples due to the fact that such samples have a much larger cross sectional area. As a result, pulse current density measurements are preferred to continuous current measurements. With a millisecond pulse duration, current densities in excess of 75000 $A/cm^2$ have been obtained for partially melted specimens at zero external field, and of

37000 A/cm$^2$ at 0.6 tesla [10].

## 2. Magnetization Critical Current

Most of the current densities reported for samples produced at the authors' laboratory and at other facilities are obtained from the magnetization measurements. This can be done only if the critical state is established in the sample. In the critical state model, first proposed by Bean [36], every region in a type II superconductor carries a critical current density $J_c$, which is determined by the local magnetic field in that region. Based on this model, the magnetization hysteresis is related to the critical current density and to the effective thickness, d, of the sample through the following expression:

$$\text{Delta } M = (1/30)\, J_c \cdot d \qquad (1)$$

where delta M is the width of the hysteresis loop, i.e. the gap between the magnetization obtained for a given magnetic field, upon decreasing and increasing the field, respectively, in emu/cm$^3$, d is the effective thickness in cm of the face of the sample normal to the applied field, and $J_c$ is the critical current density in A/cm$^2$. This expression holds when the applied field is perpendicular to the ab plane. In cases where the sample dimensions in the a and b directions ($d_a$ and $d_b$, respectively) are not the same, d is calculated as $d = (d_a \times d_b)^{1/2}$.

In the case of an applied field perpendicular to the c axis, $J_c^{ab}$ must be calculated first, and then $J_c^c$ is obtained from the following expression [12]:

$$\text{Delta } M = (J_c^c/20) \times [1 - (1/3) \times (J_c^c/J_c^{ab})] \qquad (2)$$

However, if there are local regions in the superconductor which are not yet at the critical state, (e.g. grain boundaries and weak links in sintered materials) then it is likely that the critical state is determined by one or several of the weakest regions. As mentioned above, melt processed materials have oriented grain structures without any major weak links. To ensure that the critical field is established, a plot of delta M, measured with the sample face perpendicular to the field direction should result in a straight line for different applied fields. This implies that Bean's critical state is established in these materials, and the critical current density can be estimated from the magnetization hysteresis curves. Such a plot for one of the melt processed material produced in the authors' laboratory is shown in Figure 3. The sample was in a rectangular form which was progressively cut into smaller pieces. The field was kept parallel to the c-axis. The measurements were performed with a PARC vibrating sample magnetometer and a 6-tesla SQUID.

## 3. Flux Creep Measurements

Creep measurements were performed with the applied external field either switched on or turned off. Giant flux jumps were observed when samples were charged up to very high magnetization values corresponding to more than $3 \times 10^5$ A/cm$^2$ at 4.5 K (see below).

## 4. Microstructure

The microstructure of the samples produced at the authors' laboratory was measured using techniques including SEM, EDX, and X-ray mapping and line profiling. Standard X-ray powder diffraction techniques were used for phase analysis.

## 5. Levitation Force Measurements

The levitation force, which HTC superconducting materials exercise in their interaction with magnets, has been measured by different techniques (see [37, 38, 39]). The basic principles involved in these methods are identical. The measurement consists of bringing a primary magnetic flux source to a position facing a superconducting specimen. The component of the primary flux parallel to the surface penetrates the surface, inducing shielding currents perpendicular to the applied field. The levitation force is thus the product of the current and the field. In simple terms, as the flux source is brought closer to the superconductor, more flux penetrates, resulting in a stronger shielding current, and, consequently, a stronger repulsion force. In terms of sample magnetization, the magnitude of the levitation force depends on the strength and gradient of the flux source, the size of the specimen, and the ability of the superconductor to trap the induced field, M (i.e., the sample magnetization). Thus, the levitation force is given by [40]:

$$F = M\,(dB/dz) \times (A \cdot H) \qquad (3)$$

where F is the levitation force, dB/dZ is the applied field gradient in the direction normal

to the face of the sample, A is the area of the face, and H is the thickness of the sample. The experimental set-up measurements of the force have been described in detail by Chang et al. [41].

In the dynamic force measurements, two other parameters, viz. magnetic stiffness and magnetic damping are also obtained, and it is observed that they are directly related to the flux pinning potential of the superconductor. Stiffness reflects the ability of a levitation device to supply dynamic reactive forces, and represents the slope of the force-displacement dependence, while magnetic damping reflects the ability of a levitation device to dissipate vibratory energy and is measured from the decrease in amplitude of successive oscillations after the width of the gap between a superconductor and a magnet has been changed away from its equilibrium value [42]. In a typical measurement of static force as a function of distance, a hysteresis effect similar to magnetization is obtained. The relationship between magnetization and levitation is complex, but there appears to be a direct relation between the inverse slope of the magnetization hysteresis loop (i.e. dM/dH), and the levitation force. Preliminary results indicate that when the inverse slope is zero, a large levitation is obtained, whereas negative values of the inverse slope represent lower force values. Figure 4 shows the levitation force as a function of vertical distance for two melt processed materials [43]. One of the YBCO superconductors was fabricated by Nippon Steel Corporation and the second one at the authors' laboratory. The samples were in the shape of discs, approximately 45 mm in diameter and 11 mm thick. The results show that the levitation forces of the two materials are similar in magnitude, but the magnetic damping of the material produced

at the authors' laboratories is about 3 times larger, indicating that a larger pinning potential is developed in this specimen.

## V - FLUX PINNING IN MELT PROCESSED YBCO

Pinning is caused by local fluctuations in the properties of a material which result in the free energy of the specimen depending in detail on the position of the vortices, rather than on the mean flux density. More specifically, basic pinning forces generally originate from the inhomogeneities contained in the superconductors, such as point defects, dislocation lines, precipitates, and grain boundaries [44, 45, 46]. Elastic strength associated with the distortion of the vortex line (VL) and collective as well as intrinsic pinning effects may also hinder the motion of the VL [47, 48, 49]. In the case of YBCO materials, after weak links are eliminated through melt processing, critical current densities are usually only about $10^3$ - $10^4$ A/cm$^2$ at 77 K in an applied field of H = 1 T. Further increases in $J_c$ mainly depend on the enhancement of flux pinning. In the following sections we describe several pinning mechanisms which are believed to be the most important ones in the YBCO system.

### 1. Fine-Scale Defect Pinning

The physical nature of the pinning can be made clear in certain limiting cases by splitting up the free energy of a vortex into terms which can be associated with the

condensation energy and the core of the vortex on one hand, and terms which can depend on the magnetic energy and the circulating currents on the other [47]. Especially in the HTC superconductors, as $\kappa \gg 1$ with $\kappa$ denoting the ratio between the penetration depth and the coherence length, respectively, the structure of a VL may be well described by the simplified VL model. This model is one which has a non-superconducting core of radius $\xi$, the coherence length, surrounded by a supercurrent-magnetic field region with a characteristic radius $\lambda$, the penetration depth [50, 51]. When the core is located at a non-superconducting defect, its free energy is lower than in the surrounding superconducting matrix, and the energy difference is the condensation energy. The pinning force per unit length due to the condensation energy is then estimated to be

$$p = \frac{H_c^2}{8\pi} \cdot \pi \xi^2 \cdot \frac{1}{2\xi} = \frac{H_c^2}{16} \xi \qquad (4)$$

where, $H_c$ is the thermodynamic critical field.

On the other hand, a non-superconducting defect with a dimension of $2R_d$, where $\xi < R_d \ll \lambda$, embedded in the matrix of a high temperature superconductor, may give rise to a pinning force between the defect and a vortex line due to the compression of the vortex line, in addition to the pinning force due to the condensation energy. In some cases, the action length of the pinning force due to compression of the vortex line may be much shorter than $\lambda$. In this case the pinning force induced by the compression of the vortex line may be comparable to, or even larger than, the one due to the condensation energy, depending on the size of the defect.

Usually, extremely high density defects with dimensions of about $\xi$ can be naturally introduced in thin films during their preparation. For example, STM studies of c-oriented $YBa_2Cu_3O_{6.5+x}$ films revealed a very large density of screw dislocations and stacking defects [52, 53]. This explains why $J_c$ values in these thin films are generally much higher than in the corresponding bulk materials. While dislocations or stacking faults also exist in bulk materials, it is unlikely that they can reach such a high density in such materials, especially in grain textured ones, so as to play a major role in maintaining a very high $J_c$.

In most cases, however, pinning defects can be introduced in a controlled manner. Among various defect-introducing techniques, irradiation, oxygen deficiency and chemical doping (atomic substitution) are the ones most commonly applied most for introducing fine-scale defects in HTC superconductors.

Irradiation with high energy particles, such as electrons, neutrons and protons, has proven to be very effective in flux pinning enhancement in HTC superconductors [54, 55, 56]. Because of collisions with the incident particles, some atoms in the lattice are forced to move away irreversibly from their normal positions, which then become artificial pinning centers because of the very sudden deviation of superconducting order parameters near these defects. Irradiation with different energies and types of particle incidence can produce a variety of defect sizes and patterns of distribution. As the whole irradiation process can be conveniently controlled, the resulting pinning effect can be optimized much more easily than upon using other methods. It has been demonstrated that the pinning enhancement depends heavily on the type and energy of radiation and on the

beam direction with respect to the orientation of the sample. There are even some indications of the existence of a threshold defect size for effective pinning, which is about 10 - 20 A in YBCO. Defects of this size or larger are at least $10^3$ times more effective in flux pinning than point defects [57]. It has been reported that column defects produced through irradiation, being parallel to flux vortices, have the strongest pinning effect [58]. Through irradiation, a hundred-fold increase in $J_c$ to 4.5 x $10^5$ A/cm$^2$ has already been achieved [55] at 77 K and H=1 tesla, which is almost on the same high level as $J_c$ in thin films.

It is well known that in the $YBa_2Cu_3O_{6.5+x}$ system, $YBa_2Cu_3O_{6.5}$ is non-superconducting, and as x increases, so does $T_c$, reaching its maximum with x=7. However, materials with the highest $T_c$ in this system may not perform well in flux pinning. Materials with appropriate oxygen deficiency may support high $J_c$ because these high density oxygen-deficient defects, which cause drastic changes in superconducting order parameters in their vicinity, may serve as effective pinning centers [59].

We have performed various experiments involving doping with foreign elements, in the hope that these introduced foreign elements would create local non-superconducting or lower-$T_c$ superconducting regions to serve as effective pinning centers. However, we observed that the real situation is very complicated. The foreign element chosen for doping as well as the amount of this element should be suitable for the formation of local non-superconducting or weakly superconducting regions rather than for the dopant to be deeply submerged by the superconducting proximity effect or to suppress too much the overall superconductivity of the matrix material. Besides, the processing involved in the

doping experiment should be tailored to accommodate the introduction of the foreign element. For example, for each element there is a certain temperature range in which the element reaches its maximum solubility in the matrix material, and if the sample is held at a certain lower temperature too long, the foreign atoms tend to segregate and accumulate at the grain boundaries. In this case the introduction of the dopant may cause serious weak-link problems instead of being beneficial.

Among the various doping experiments performed by us, doping with Pr, for instance, is typical. It has been reported [60, 61, 62] that $PrBa_2Cu_3O_x$ is a non-superconductor with very high resistivity at low temperatures; it has the same orthorhombic structure as superconducting $YBa_2Cu_3O_x$ and its a-b lattice constants are within 1.5% of those of $YBa_2Cu_3O_7$. Pr therefore has high solubility in the $YBa_2Cu_3O_x$ system. Moreover, superconductivity in $YBa_2Cu_3O_x$ is known to be strongly suppressed by the substitution of Pr for Y [63, 64], e.g., in $Pr_yY_{1-y}Ba_2Cu_3O_x$, with $y = 0.3$, the transition temperature $T_c$ becomes 57 K. Accordingly, it was expected that doping of Pr in trace amounts would result in a wide distribution of $Pr^{3+}$ ions throughout the material, causing the formation of local defect regions to serve as effective pinning centers. We conducted the Pr-doping experiments through use of partial-melt-growth processing at an oxygen pressure of about 25 psi, taking care to use a carefully adjusted cooling rate at high temperature, because the cooling rate is was very important for effective doping.

Figure 5 shows a hysteresis curve for a grain-textured bulk sample of $Pr_{0.01}Y_{0.99}Ba_2Cu_3O_x$. The measurement was performed with the applied field being parallel to the c-axis. Measurements of a.c. susceptibility showed that the sample has a

$T_c$ of about 90 K. Magnetization values in Figure 5 were converted to $J_c$ values using Bean's critical state equation, as shown in Figure 6. Usually, bulk superconductors show a monotonically decreasing magnetic hysteresis as well as critical current density with increasing magnetic field at constant temperature. However, Figures 5 and 6 show an unusual behavior, with the hysteresis and, consequently, the critical current density dropping to a minimum, then rising, instead of dropping, up to H = 0.7 tesla. Figure 7 illustrates that the magnetization at 77 K continues to rise to a maximum at about 1 tesla before falling to zero at about 3.5 tesla.

Jin *et al.* [65] used a technique which is based on decomposing the $YBa_2Cu_4O_x$ precursor into $YBa_2Cu_3O_7$ + CuO. As Cu atoms have to come out from every unit cell, very high density of fine-scale defects may therefore be built up inside grains. By this approach they observed an increase in intra-grain $J_c$ by a factor of ten over the values obtained in typical $YBa_2Cu_3O_7$ samples.

The combination of doping and grain-texturing is complicated. Excessive doping may suppress the overall superconductivity, and may also introduce new weak links. We are conducting studies of doping and grain-texturing in a systematic manner to optimize the current and pinning potential.

2- Large-scale defect pinning

Defects with dimensions much larger than the coherence length $\xi$ may also effectively enhance flux pinning because of their large-scale boundaries, across which there is a sharp change in the parameters of superconductivity. In polycrystalline materials, this

type of boundary defects can exist in various forms, such as isolated weak links at the grain boundaries, isolated microcracks, and boundaries between the superconducting matrix and very weakly superconducting or non-superconducting precipitates and inclusions, etc. The basic pinning forces involved can be divided into two types, one due to the vortex core pinning interaction, corresponding to the condensation energy, at the boundary, and the other one resulting from magnetic pinning interaction, i.e., the image pinning force, near the boundary. $J_c$ due to large-scale boundary pinning is found to be

$$J_c(B,T) = 1.28\times10^3(1+C_0)S_v H_c^2 \xi \frac{(1-\frac{B}{B_{c2}})}{\sqrt{B_r+B}}, \qquad (5)$$

where the units of the variables which appear in the equation are $cm^{-1}$ for $S_v$, cm for $\xi$, and Gauss for $H_c$ and B. $S_v = d^2/l^3$, where d is the average dimension of the effective boundary defects and $l$ their average spacing. $B_r$ is the average remanent magnetic flux density. $C_o$ is an uncertainty factor, ranging from 1 to 8, depending on the structure of the boundary, particularly on its smoothness and the thickness of its transition layer.

Since image force occurs near the boundary, it has to be balanced by the Lorentz force resulting from the surface layer current near the boundary. However, because of the demagnetization effect, the local field is usually very sensitive to fluctuations of roughness of the boundary, and so is the surface layer current. An extremely thin interface transition layer is also essential for strong boundary pinning, since it leads to a very sharp reduction of the superconducting order parameter. Obviously, if the introduced boundaries fail to meet these conditions with respect to smoothness and

thickness, then the positive role of large-scale boundary defects on pinning can hardly be observed. This might be the major reason why at the present time opinions on the effectiveness of large-scale defect pinning in HTC superconductors are very conflicting.

Through our melt processing techniques, especially when high oxygen pressure is used, second phase inclusions with high smoothness and sharp transition interface have been produced. It has been observed that the amorphous layer between a $Y_2BaCuO_5$ inclusion and the $YBa_2Cu_3O_7$ matrix may be as thin as 1nm [66]. As an example, Fig. 8 shows both the measured value and predicted value, based on the equation given above for $J_c$, of $J_c$ as a function of the applied field at 77 K for a YBCO sample produced through pressurized melt growth processing. $S_v$ in this case was estimated to be about 350/cm on the basis of an SEM study. The fairly good agreement between the two curves of $J_c$ suggests that in this case large-scale boundary defect pinning do play an important role in the enhancement of $J_c$.

The enhancement of flux pinning through the introduction of other types of second phase inclusions or precipitates has also been reported. Such second phases have included as $BaSnO_3$ and $BaTiO_3$ in $YBa_2Cu_3O_7$ [67, 68] and $Ca_2CuO_3$ and $CaSrPbO_4$ in Bi-Sr-Ca-Cu-O systems [69, 70]. Although the number of inclusions per unit volume can be increased over a certain range, and so can $S_v$, it is difficult to raise $J_c$ to a level of $10^6$ A/cm$^2$ by increasing $S_v$ alone. For example, to achieve $J_c = 5 \times 10^5$ at 77 K and H = 1 tesla in $YBa_2Cu_3O_7$ through $Y_2BaCuO_5$ inclusions, $S_v$ has to be as large as $2.4 \times 10^3$ /cm, even after setting $C_o$ in Eq. 5 equal to the maximum value of 8 for an optimized

estimate. It means that even if the average dimension of the $Y_2BaCuO_5$ inclusions can be controlled to be as small as 2.5 $\mu$m, the total volume percentage of the $Y_2BaCuO_5$ phase still has to be as high as 60% for $S_v$ to reach $2.4 \times 10^3$ /cm. Such a large amount of non-superconducting phase will certainly make the grain-texturing very difficult, even without mentioning a serious decrease in the effective extent of the superconducting region due to the presence of the large amount of $Y_2BaCuO_5$ inclusions.

## VI - FLUX CREEP IN MELT PROCESSED YBCO

Inside type II superconductors, supercurrent can exist because of flux pinning. However, the flux lines may jump over pinning barriers due to thermal activation, which, according to the flux creep model of Anderson [71], leads to a jump rate of $\nu$,

$$\nu = \nu_o e^{-U_o/kT} \qquad (6)$$

Here $\nu_o$ is a characteristic attempt frequency, and $U_o$ is the activation energy. $U_o$ at low temperature ($T \sim 10$ K) has been estimated to be of the order of 1 ev for conventional superconductors [72], but only about 0.01 - 0.03 ev for normally sintered or single-crystal high-$T_c$ superconductors and high-$T_c$ films [72, 73, 74]. When the temperature increases, the situation becomes worse, not just because of the increasing thermal energy, but also because of the decreasing value of $U_o$, which leads to giant flux

creep in HTSC at 77 K [73]. This caused at one time a serious concern about the usefulness of HTSC materials [75]. Later researchers, however, found that in certain types of "dirty" $YBa_2Cu_3O_x$ single crystals, $U_o$ at 77 K may be as high as 0.1 - 0.3 ev [76], and in grain-textured Y-Ba-Cu-O materials $U_o$ may be as high as 0.7 ev [77]. In the cases of the samples prepared through our pressurized-partial-melt processing technique, $U_o$ values exceeding 1.0 ev have been obtained at 77 K.

$U_o$ is usually defined as the activation energy for flux creep which occurs at $J \approx J_c$, namely when the vortex lattice is in the critical state. A fully critical state can easily be achieved by charging the sample with a sufficiently high magnetic field, and then completely withdrawing the applied field. The value of $U_o$ can then be obtained by measuring the relaxation of the remanent magnetization, $M_r(t)$. In experiments carried out in the authors' laboratory, after cooling to 77 K, the sample was charged for 10 minutes with a field of 0.75 tesla in a direction either parallel or perpendicular to the c axis. When the field was decreased to zero, the remanent magnetization in both cases reached the saturation value. The magnetization was then measured every 8 seconds using a vibrating sample magnetometer. About 100 - 200 s after the charging field was decreased to zero, the relaxation rate became relatively stabilized, and then a logarithmic decay of $M_r(t)$ was obtained in both cases, as shown in Figs. 9A and 9B. The conventional flux creep relation [78,79] is given by

$$M(t) = M_0 \left[ 1 - \frac{kT}{U_{eff}} \ln \frac{t}{t_0} \right] \qquad (7)$$

An effective activation energy $U_{eff}$ can be obtained from the slope of the curves of $M_r/M_{r_o}$ vs. ln(t). Here $t_o$ is the vortex-hopping attempt time and $M_o$ is the initial remanent magnetization. According to this equation, $U_{eff}$ in the case of pressurized-melt-textured YBCO was found to have values of about 1.3 ev or 1.5 ev, corresponding to the cases of the charging field being parallel to the c axis or perpendicular to the c axis, respectively.

At the present time, the exact physical implications of $U_{eff}$ have not yet been completely elucidated. It is widely believed that $U_{eff}$ scales with the pinning potential, and any increase in pinning force will effectively increase $U_{eff}$. However, the real situation is much more complicated. Although $J_c$ is undoubtedly proportional to the pinning force, recent experiments on Y-Ba-Cu-O materials have shown that in single-crystal materials $J_c$ or the pinning force can be increased by two orders of magnitude through proton irradiation, while $U_{eff}$ increases by less than 25% [76]. In melt-textured bulk samples, $U_{eff}$ remains unchanged to within $\sim$ 10% as $J_c$ or the pinning force increases by a factor of 15 through neutron irradiation [62]. It is therefore clear that, at least in high $T_c$ superconductors, $U_{eff}$ mainly depends on the structure of the pinning barriers rather than on the total pinning force density. Strong irradiation can introduce strong point pinning as well as strong line pinning, and consequently may raise $J_c$ dramatically. In melt-textured samples, there are many large boundary defects caused by inclusions and isolated weak links, which are rarely seen in single-crystal samples. The large increase in $U_{eff}$ in the melt-textured samples implies that these large boundary

defects are responsible for the high values of $U_{eff}$.

Although very high values of $J_c$ may be achieved by introducing defects using various approaches such as irradiation, and, probably, chemical doping, it seems likely that introduction of large amount of boundary defects is very important for obtaining a high effective activation energy for flux creep. Therefore, these different approaches should be combined, and incorporated in the design of methods intended to provide improvement in both the value of the critical current density and its stability.

Flux jump is an extension of flux creep that normally occurs near critical levels of current where the creep rate is enhanced and the superconductor is most susceptible to thermal fluctuations. Flux jumps give rise to massive disturbances which can produce enough heat to cause large sections of the device to become normal. Figure 10 represents a M-H curve at 4.5 K for a melt processed sample which is doped with excess yttrium and platinum. The flux jumps can clearly be seen when the external field produces supercurrents in the excess of $3 \times 10^5$ A/cm$^2$. The interesting feature of this material is that flux jumps are arrested relatively slowly after they are occurred, which makes the system unstable.

For stability, the ratio of cooling to joule heating must be large enough so that the superconductivity can be regained immediately after the jump. In conventional low temperature superconductors, the flux jump process is avoided by embedding filaments of superconductor in metal matrix for better heat conduction. However, HTC wires are still far away from reaching their potentially high current densities (except bismuth wires below 20 K), let alone multifilamentry forms. Therefore the flux jump problem has

serious implications for these materials. Fortunately, for HTC materials the flux jump field is one to two orders of magnitude larger than for conventional superconductors [80]. As a result, the requirement for the use of multifilamentry conductors is greatly relaxed, and bulk materials become an attractive option for many applications such as strong magnets.

## VII - MAGNETIZATION ANOMALIES IN MELT PROCESSED YBCO

In certain YBCO materials doped with various second phases, we have observed a peak in irreversible magnetization preceded by a minimum after the first maximum in the reversible region (see above). Such behavior has been also reported for single crystals of YBCO [81, 82, 83]. This phenomenon has been attributed to the oxygen defects. The general hypothesis is that the oxygen deficient regions have lower $T_c$ and $H_{c2}$ values than the matrix. At low fields these regions are either proximity- or Jospheson- coupled, but higher fields will drive them normal, and thus they become much more effective pinning centers. At still higher fields the oxygen deficient regions can link up and form intra-granular granularity which will render the system normal.

The anomalous behavior in doped-melt processed YBCO superconductors appears to be similar to the corresponding phenomenon in single crystals. Such behavior has been observed for a variety of dopants, including Pr, Bi, V, and In. Even though no firm

consensus exists concerning the formation of these peaks in polycrystalline materials, the best explanation at this time would be a similar argument to the one presented above for single crystals. Here, instead of oxygen defects we would consider a region of weak ***coupling effect*** between the dopant and the matrix, which is formed in the Pr-doped samples described in the pinning section.

Unlike Pr-doped materials, we did not see any obvious anomalous phenomena in the pure YBCO analogs which were produced under the same processing conditions. Since both types of samples were well oxygenated, we concluded that the oxygen deficient defects are not the major cause for the anomalous phenomena observed in the case of the $Pr_{0.01}Y_{0.99}Ba_2Cu_3O_x$ material, but that these phenomenon are related to the doping with $Pr^{3+}$ ions. We believe that suppression of superconductivity in the coupling regions around the $Pr^{3+}$ ions at high fields is the major reason for this unusual behavior. As was described above in the discussion of flux pinning, the pinning effect corresponds to the fluctuation of superconductivity in the material. The smaller activity of the pinning effect at lower fields, shown in Figure 6, suggests that at lower fields the local regions around the widely distributed $Pr^{3+}$ ions are well coupled in superconductivity with the matrix (see Figure 11a). In other words, superconductivity in and near these defect regions may not seriously fluctuate because of the coupling effect. However, superconductivity in these defect regions is still relatively weak compared with that in the matrix (see Figure 11). Moreover, the superconducting coupling effect not only is sensitive to the magnetic field, but it is also a function of temperature. Consequently, with the field increasing, the weak superconducting regions in the matrix become more

weakly superconducting or even non-superconducting, and the weakly superconducting or non-superconducting regions become larger. This is expected to make the defect regions more effective in serving as pinning centers. This results in an increase in hysteresis and in $J_c$ with increasing magnetic field as shown previously in Figures 5 and 6, respectively. The coupling effect shifts to higher fields when the temperature is lowered, indicating the weak superconducting coupling regions become superconducting, and larger fields are required to drive the material into the normal state, consistent with the way in which weak link behavior varies with temperature. This effect is illustrated in Figure 12 which shows the peak is progressively shifted to higher fields and disappears completely at 10 K. Similar anomalous behavior has been observed with several other dopants. The magnetization curves for the cases of doping with bismuth and with indium are shown in Figures 13 and 14, respectively. It is worth noting that, when the crystalline lattice matching of the dopant phase is not as good as in the case of Pr, which is probably the case upon doping with Bi or In, a more diffuse coupling region is expected to form. By increasing the amount of doping the coupling regions may grow in volume until they become interconnected, resulting in the formation of weak links and degradation of overall superconductivity. In addition, we have observed that the peaks in magnetization obtained with different dopants are observed at different intensities of applied field. We believe that the displacement of the peak position upon changing dopants is due to the fact the each dopant may couple differently in the host superconducting matrix. We are currently conducting systematic doping and oxygenation studies on melt processed YBCO materials. By controlling the field dependence of the

peak, we hope to be able to select materials that can operate at their maximum magnetization at a given non-zero external applied magnetic field.

## ACKNOWLEDGEMENTS

The authors are grateful to S. A. Olszowka for preparing the manuscript. This study was supported by the National Aeronautics and Space Administration under Contract No. NAG 5-1017.

## References


1) J. G. Bednorz, K. A. Muller: Z. Phys, 1986, B64, 189.

2) M. K. Wu, J. R. Ashburn, C. J. Torng, P. H. Hor, R. L. Meng, L. Gao, Z. J. Huang, Y. Q. Wang, And C. W. Chu: Phys. Rev. Lett., 1987, 58, 908.

3) H. Maeda et al.: Japan J. Appl. Phys., 1988, 27, L209.

4) Z. Z. Sheng and A. M. Hermann: Nature, 1988, 332, 55.

5) L. N. Shehata: J. Low Temp. Phys., 1990, 78, 25.

6) R. B. Laibowitz, R. H. Koch, P. Chaudari, and R. J. Gambino: Phys. Rev. Lett., 1987, B35, 8821.

7) L. F. Schneemeyer, E. M. Gyorgy, and J. V. Waszczak: Phys. Rev. B, 1987, 36, 8804.

8) S. Jin, T. H. Tiefel, R. C. Sherwood, M. E. Dowis, R. B. van Dover, G. W. Kammlot, R. A. Fastnacht, and H. D. Keith: Appl. Phys. Lett., 1988, 52, 2074.

9) H. Hojaji, K. A. Michael, A. Barkatt, A. N. Thorpe, M. F. Ware, I. G. Talmy, D. A. Haught, and S. Alterescu: J. Mater. Res. Soc., 1989, 4, 1.

10) K. Salama, V. Selvamanickam, L. Gao, and K. Sun: Appl. Phys. Lett., 1989, 54, 2352.

11) M. Murakami, M. Morita, and N. Koyama: Jpn. J. Appl. Phys., 1989, 28, L1125.

12) S. Hu, in Ph.D. Dissertation, Catholic University of America, Washington, DC, 1991.

13) M. Morita, M. Tanaka, T. Sasaki, M. Hashimoto, and K. Sawano, Proceeding of M2-S, Physica C, (to be published).

14) H. Hojaji, A. Barkatt, S. Hu, K. A. Michael, A. N. Thorpe, I. Talmy, D. A. Haught, and S. Alterescu: Mat. Res. Bull., 1990, 25, 765-777.

15) M. Tashiki and S. Takahashi: Solid State Cummunication, 1989, 70, 291.

16) P. Berghuis, P. H. Kes, B. Dam, G. M. Stollman, and J. Van Bentum: Physica C, 1990, 167, 348.

17) M. Murakami, M. Morita, K. Doi, and K. Miyamoto: Jpn. J. Appl. Phys., 1989, 28, 1189.

18) H. Hojaji et al.: J. Mater. Res., 1990, 5, 4, 721.

19) L. Civale, A. D. Marwick, M. W. McElfresh, T. K. Worthington, A. P. Malozemoff, F. Holtzberg, J. R. Thompson, and M. A. Kirk: Phys. Rev. Lett., 1990, 65, 1164.

20) L. Civale, A. D. Marwick, T. K. Worthington, M. A. Kirk, J. R. Thompson, L. Krusin-Elbaum, Y. Sun, J. R. Clem, and F. Holtzberg: Phys. Rev. Lett., 1991, 67, 648.

21) J. Mannhart, D. Anselmetti, J. G. Bednorz, C. Gerber, K. A. Muller, and D. G. Schlom: Superconductors, Churchill College, Cambridge, England, 1991 (pre-print).

22) R. S. Roth, K. L. Davis, and J. R. Dennis: Adv. Ceram. Mat., 1987, 2, 3B, 303.

23) M. Nevriva, E. Pollert, J. Sestek, L. Matejkova, and A. Triska: Physica C, 1988, 133-135, 377.

24) T. Aselage and K. Keefer: J. Mater. Res., 1988, 3, 1279.

25) K. Yamaguchi et al.: Physica C, 1990, 169, 289-293.

26) K. Dembinski, M. Gervais, P. Odier, and J. P. Coutures: J. of the Less Common Metals, 1990, 164-165, 177-186.

27) R. L. Meng, P. H. Hor, and C. W. Chu, Presentation in Mater. Res. Soc. Fall Meeting, Boston, Massachusetts, 1991.

28) T. H. Tiefel, S. Jin, G. W. Kammlott, and R. A. Fastnacht, Presentation in Mater. Res. Soc. Fall Meeting, Boston, Massachusetts, 1991.

29) Z. Lian, Presentation at TMS Annual Meeting, 3rd Int. Symp. on High-Temp.

Superconductors, New Orleans, Louisiana, 1991.

30) H. Fujimoto, M. Murakami, S. Gotoh, N. Koshizuka, T. Oyama, Y. Shiohara, and S. Tanka, Advances in Superconductivity II, Springer-Verlag, Tokyo, 1989.

31) S. Hu, H. Hojaji, A. Barkatt, M. Boroomand, M. Hung, A. C. Buechele, A. N. Thorpe, D. D. Davis and S. Alterescu, accepted for publication in the J. Mat. Res.

32) H. Hojaji, A. Barkatt, S. Hu, K. A. Michael, A. N. Thorpe, I. G. Talmy, D. A. Haught, and S. Alterescu: Mat. Res. Bull., 1990, 25, 1025-1031.

33) M. Itoh, M. Saitoh, K. Oka, and H. Unoki: Jap. J. of Appl. Phys., 1988, 27, 9, L1634.

34) T. J. Folkerts, M. J. Kramer, K. W. Dennis and R. W. McCallum: preprint.

35) T. Yamamoto, M. Stubicar, S. K. Chan, J. G. Lu, T. R. S. Prasanna, and R. C. O'Handley: Mater. Sci. and Engineering, 1991, A133, 127-131.

36) C. P. Bean: Phys. Rev. Lett., 1962, 8, 250-253.

37) F. C. Moon, U. S. Patent 4,931,732 June 1990.

38) T. H. Johansen, Z. J. Yang, H. Bratsburg, G. Helgesen, and A. T. Skjeltorp: Appl. Phys. Lett., 1991, 58, 2, 179-181.

39) V. V. Nemoshkalenko, E. H. Brandt, A. A. Kordyuk, and B. G. Nikitin: Physica C, 1990, 170, 481-485.

40) H. Hojaji, A. Barkatt, and A. N. Thorpe: Jap. J. Appl. Phys, 1990, 29, 7, 1257-1258.

41) P. Z. Chang, F. C. Moon, J. Hull, and T. Mulchay: J. Appl. Phys., 1990, 67, 4358.

42) F. C. Moon and P. Z. Chang: Appl. Phys. Lett., 1990, 56, 397-399.

43) D. Rao, presented and the DARPA Workshop, Los Alamos, 1991.

44) H. Kronmuller, *International Discussion Meeting on Flux Pinning Superconductors*, edited by P. Haasen and H. C. Freyhardt (Goltze-Druck, Gottingen, 1975), p. 1.

45) R. B. Van Dover, E. M. Gyorgy, A. E. White, L. F. Schneemeyer, R. J. Feilder, and J.

V. Waszczak: Appl. Phys. Lett., 1990, **56**, 2681.

46) O. F. Schlling, Y. Yang, C. R. M. Grovenor and C. Beduz: Physica C, 1990, **170**, 123.

47) A. M. Campbell and J. E. Evetts: Advan. Phys., 1972, **21**, 199.

48) L. Schimmele, H. Kronmuller, and H. Teichler: Phys. Status Solidi B, 1988, **147**, 361.

49) B. I. Ivlev and N. B. Kopnin: Phys. Rev. Lett., 1990 **64**, 1828.

50) D. Saint-James, E. J. Thomas, and G. Sarma, *Type II Superconductivity* (Pergamon Press, N.S.W., 1969), p. 64.

51) H. Wu, W. Guan, and H. Li, *Superconductivity - Type II Superconductivity and Weak Link Superconductivity* (Chinese Press of Science, Beijing, 1979), p. 15.

52) M. Hawley, T. D. Raistrick, J. G. Beery, and R. J. Houlton: Science, 1991, **251**, 1581.

53) C. Gerber, D. Anselmetti, J. G. Bednorz, J. Mannhart, and D. G. Schlom: Nature, 1991, **350**, 279.

54) T. Shiraishi, Kato, J. Kuniya: Jpn. J. Appl. Phys., 1989, **28**, L807.

55) R. B. van Dover, E. M. Gyorgy, L. F. Schneemeyer, J. W. Mitchell, K. V. Rao, R. Puzniak, and J. V. Waszczak: Nature **342**, 1989, 55.

56) R. B. van Dover, E. M. Gyorgy, L. F. Schneemeyer, A. E. White, S. Glarum, R. J. Felder, and J. V. Waszczak: Appl. Phys. Lett., 1990, **56**, 2681.

57) J. Bechtold, Y. Y. Xue, Z. J. Huang, E. V. Hungerford, P. Hor, C. W. Chu, X. K. Maruyama, H. Backe, F. R. Buskirk, S. M. Connors, D. D. Snyder, Y. C. Jean, and J. W. Farmer, preprint.

58) L. Civale *et. al.*: Phys. Rev. Lett., 1991, **67**, 648.

59) J. M. Seuntjens, M. Daeumling, and D. C. Larbalestier, to be published.

60) C. Infante, M. K. El Mously, R. Dayal, M. Husain, S. A. Siddiqi, and P. Ganguly: Physica C, 1990, **167**, 640.

61) C. L. Jia, B. Kabius, H. Soltner, U. Poppe, and K. Urban: Physica C, 1990, **167**, 463.

62) J. L. Peng, P. Kalvins, R. N. Shelton, H. B. Radousky, P. A. Hahu, and L. Bernandez: Phys. Rev. B, 1989, **40**, 4517.

63) V. A. Voloshin: Physica C, 1990, **168**, 506.

64) J. J. Neumeier, M. B. Maple and M. S. Torikachvili: Physica C, 1988, **156**, 574.

65) S. Jin, T. H. Tiefel, S. Nakahara, J. E. Graebner, H. M. O'Bryan, R. A. Fastnacht, and G. W. Kammlott: Appl. Phys. Lett., 1990, **56**, 1287.

66) K. Yamaguchi, M. Murakami, H. Fujimoto, S. Gotoh, N. Koshizuka, and S. Tanaka: Jpn. J. Appl. Phys., 1990, **29**, L1428.

67) P. McGinn, W. Chen, N. Zhu, L. Tan, C. Varanasi, and S. Sengupta: Appl. Phys. Lett., 1991, **59**, 120.

68) O. F. Schilling, Y. Yang, C. R. M. Grovenor, and C. Beduz: Phys. C, 1990, **170**, 123.

69) T. Hikata, K. Sato, and H. Hitotsuyanagi: Jpn. J. Appl. Phys., 1989, **28**, L82.

70) D. Shi, M. S. Boley, U. Welp, J. G. Chen, and Y. Liao: Phys. Rev., 1989, **B40**, 5255.

71) P. W. Anderson: Phys. Rev. Lett., 1962, **9**, 309.

72) Ming Xu and Donglu Shi: Physica C, 1990, **168**, 303.

73) Y. Yeshurun and A. P. Molozemoff: Phys. Rev. Lett., 1988, **60**, 2202.

74) S. Hatta, Y. Ichikawa, H. Adachi, and K. Wasa: Jpn. J. Appl. Phys., 1989, **28**, L422.

75) Anil Khurana: Phys. Today, p. 17, March 1989.

76) L. Civalk, A. D. Marwick, M. W. McElfresh, T. K. Worthington, P. A. Malozemoff, F. H. Holtzberg, J. R. Thompson, and M. A. Kirk: Phys. Rev. Lett., 1990, **65**, 1164.

77) M. Murakami, M. Morita, and N. Koyama: Jpn. J. Appl. Phys., 1989, **28**, L1754.

78) A. M. Campbell and J. E. Evetts: Adv. Phys., 1972, **21**, 199.

79) P. W. Anderson and Y. B. Kim: Rev. Mod. Phys., 1964, **36**, 39.

80) S. L. Wipf, SSS90, Nov 13-15, 1990, Yokohama, Japan.

81) H. Kupfer, I. Apfelstedt, R. Flukiger, C. Keller, R. Meier-Hirmer, B. Runtsch, A. Turowski, U. Weich, and T. Wolf: Cryogenics, 1989, 29, 286.

82) Y. Xu, M. Svenaga, A. R. Moodengbaugh, and D. O. Welch: Phys. Rev. B, 1990, 40, 10882.

83) M. Daeumling, J. M. Seuntjens and D. C. Larbalestier: Nature, 1990, 346, 332.

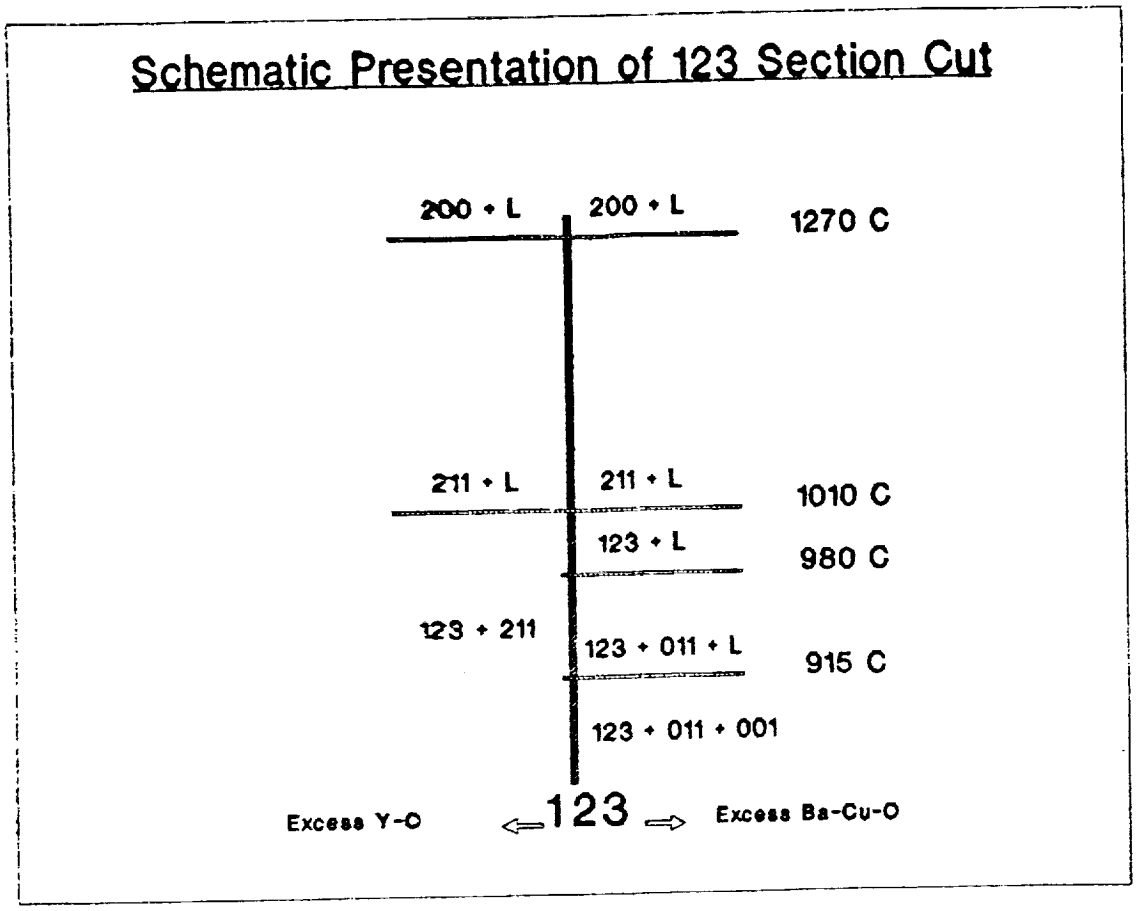


Fig. 1 Schematic presentation of the 123 section of the YBC: phase diagram.

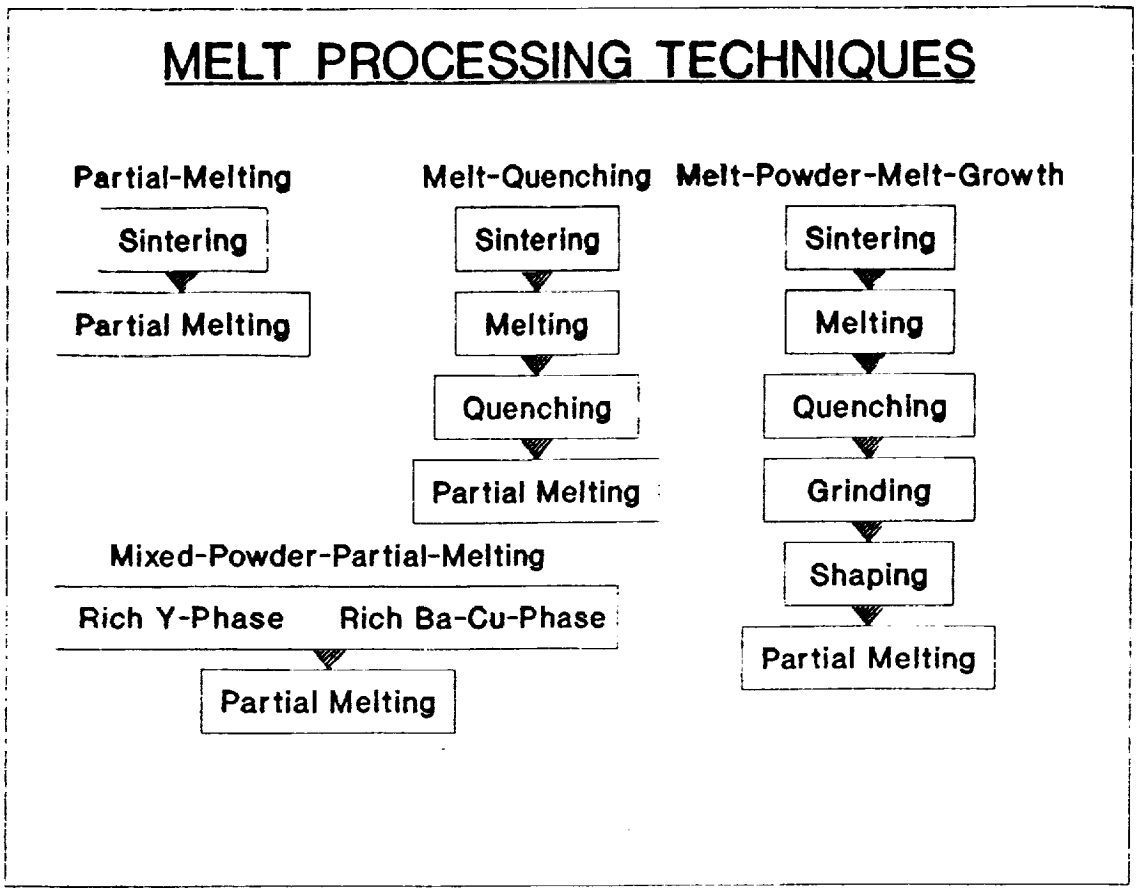


Fig. 2 Flow chart of the different melt processing techniques

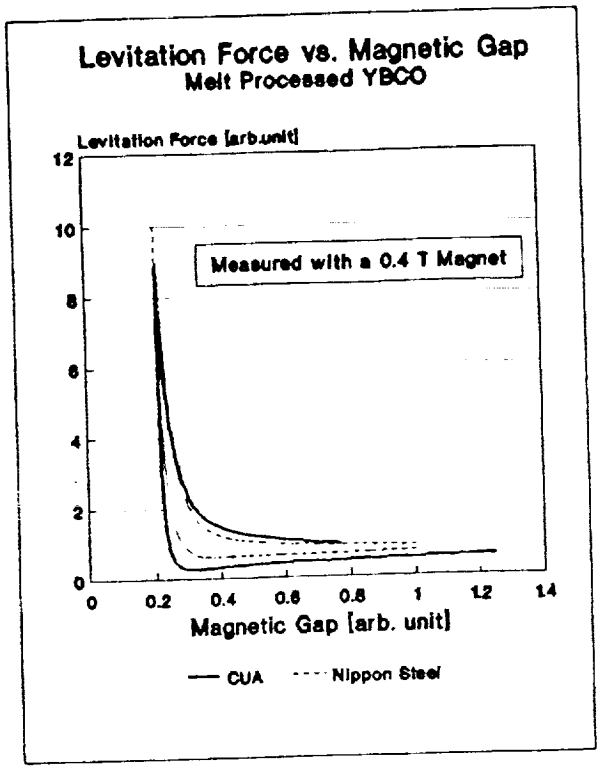


Fig. 4A Levitation force as a function of the magnetic gap (gap between the superconductor and the magnet) for two melt processed Y-Ba-Cu-O samples from Nippon Steel and the authors' laboratory

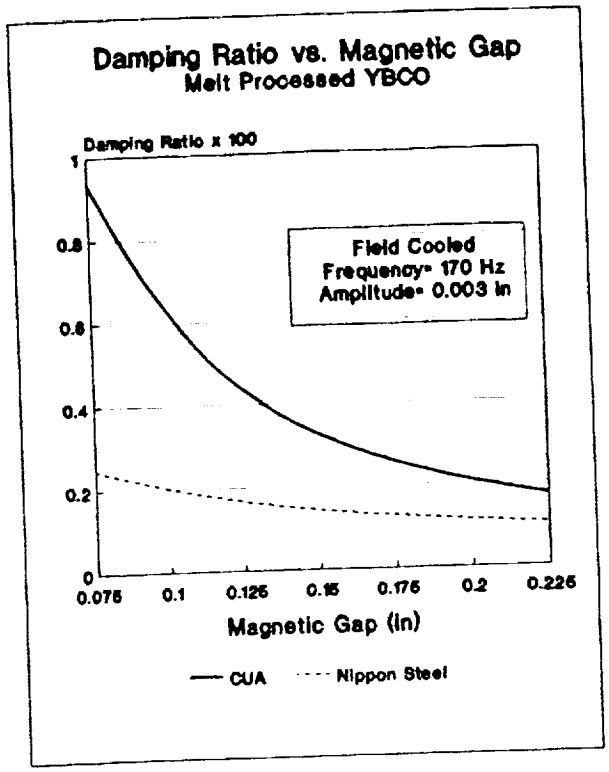


Fig. 4B Magnetic damping of the two materials in (A).

Data from D. Rao, MTI

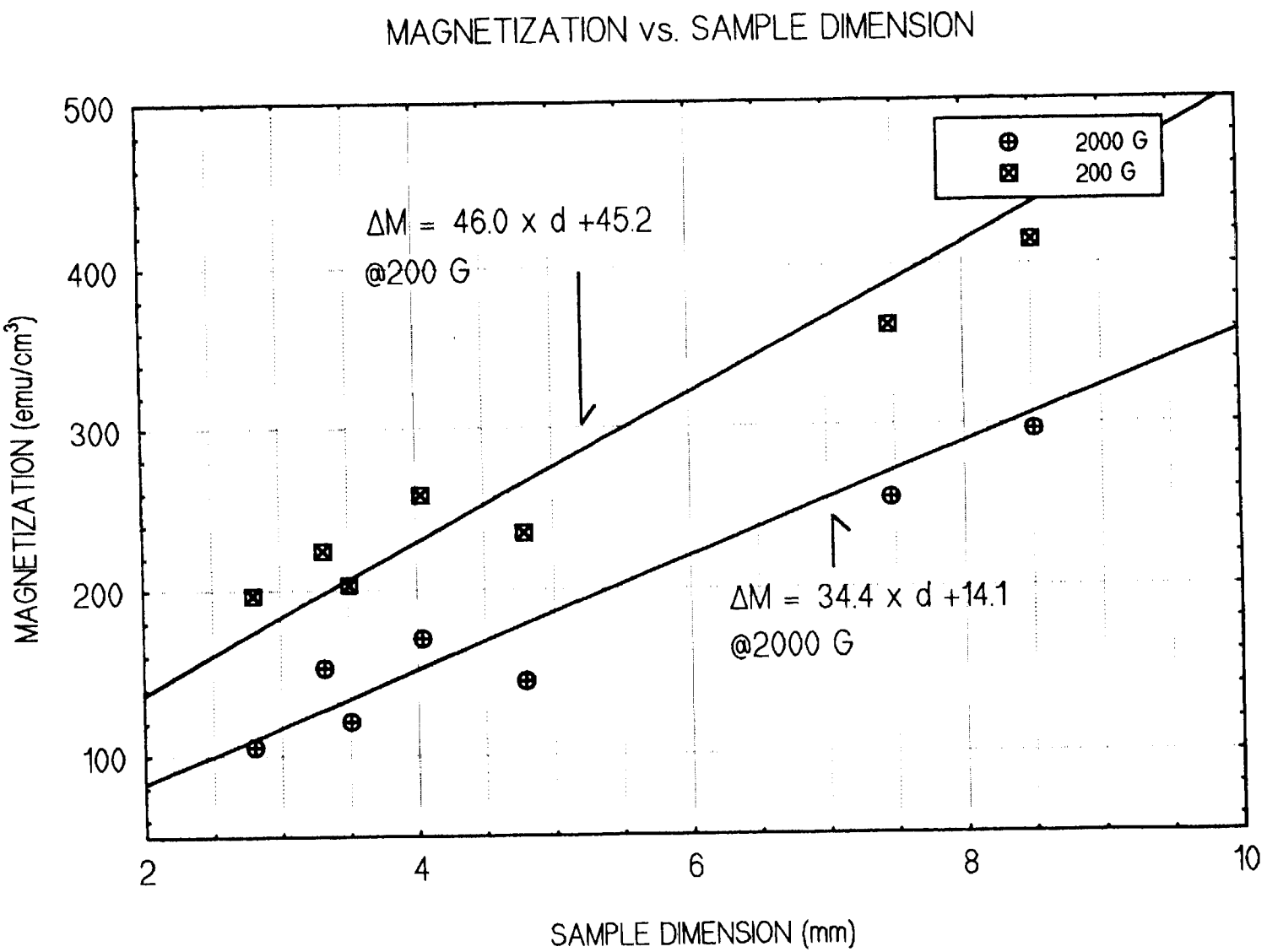
MAGNETIZATION vs. SAMPLE DIMENSION
2000 G
200 G
ΔM = 46.0 x d +45.2
@200 G
ΔM = 34.4 x d +14.1
@2000 G
MAGNETIZATION (emu/cm³)
SAMPLE DIMENSION (mm)
500
400
300
200
100
2
4
6
8
10

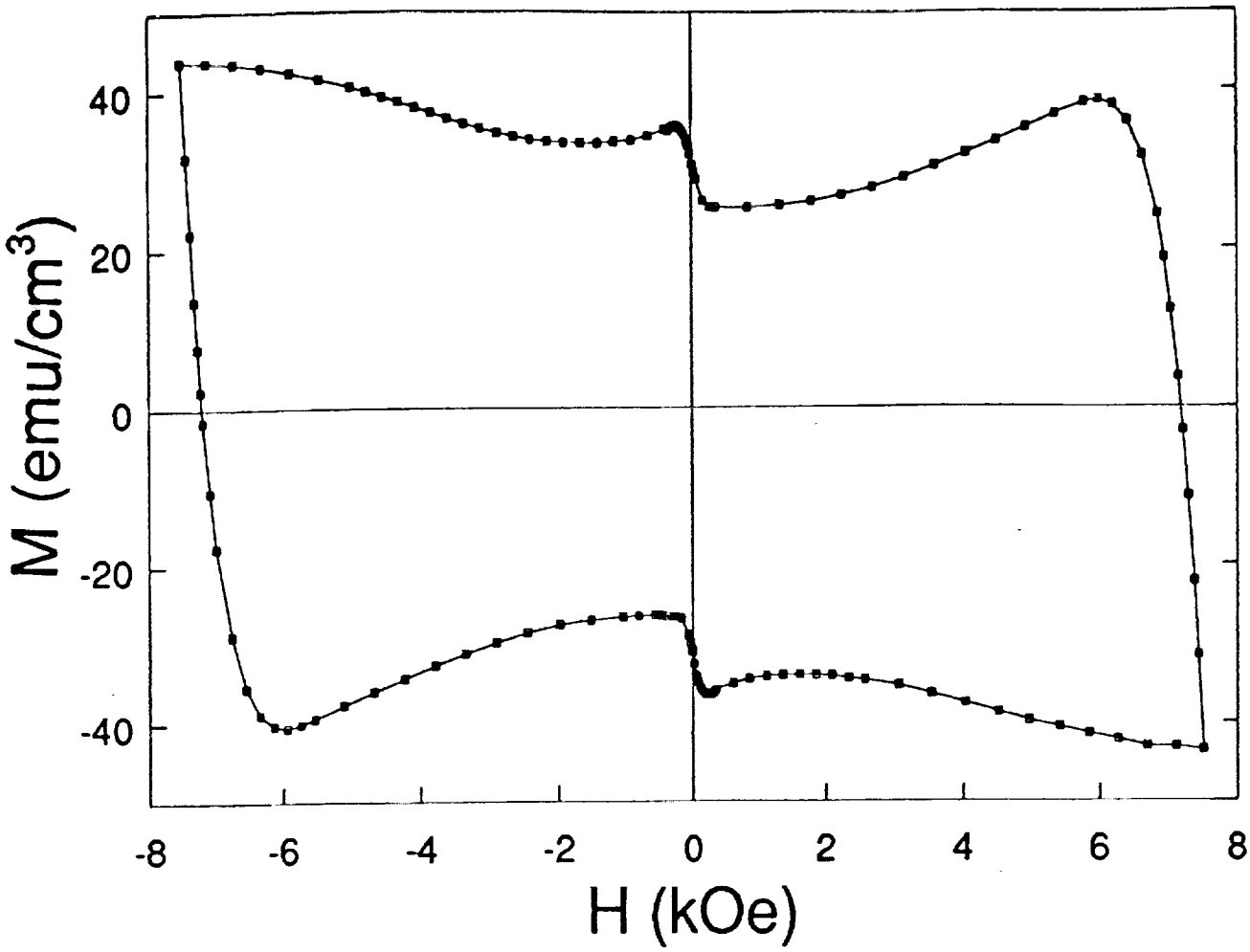


Fig. 5 Magnetic hysteresis curve at 77 K for a melt processed Pr-Y-Ba-Cu-O sample.

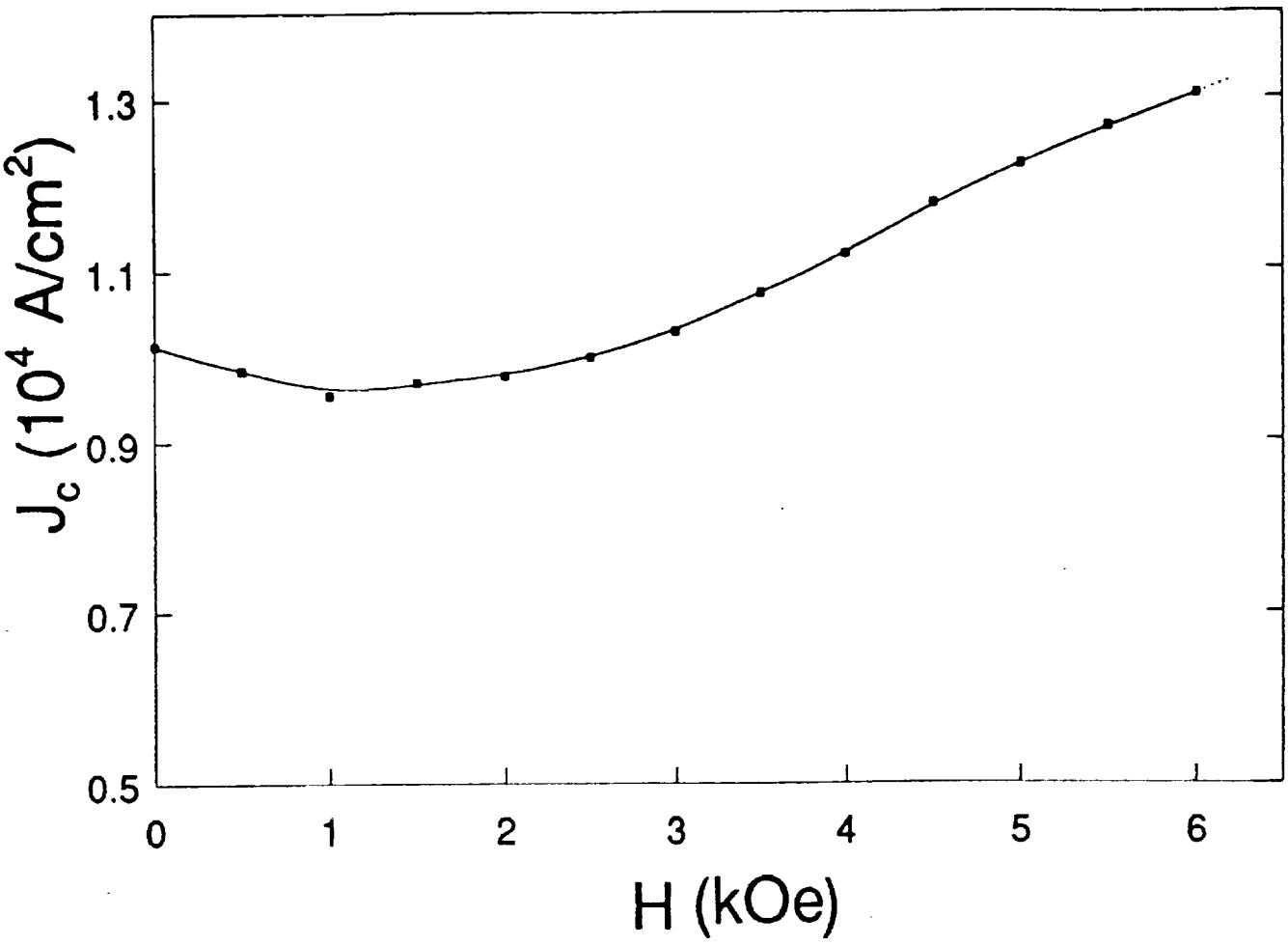


Fig. 6 $J_c$, converted from the data in Fig. 5, as a function of the applied field at 77 K for the same Pr-Y-Ba-Cu-O sample.

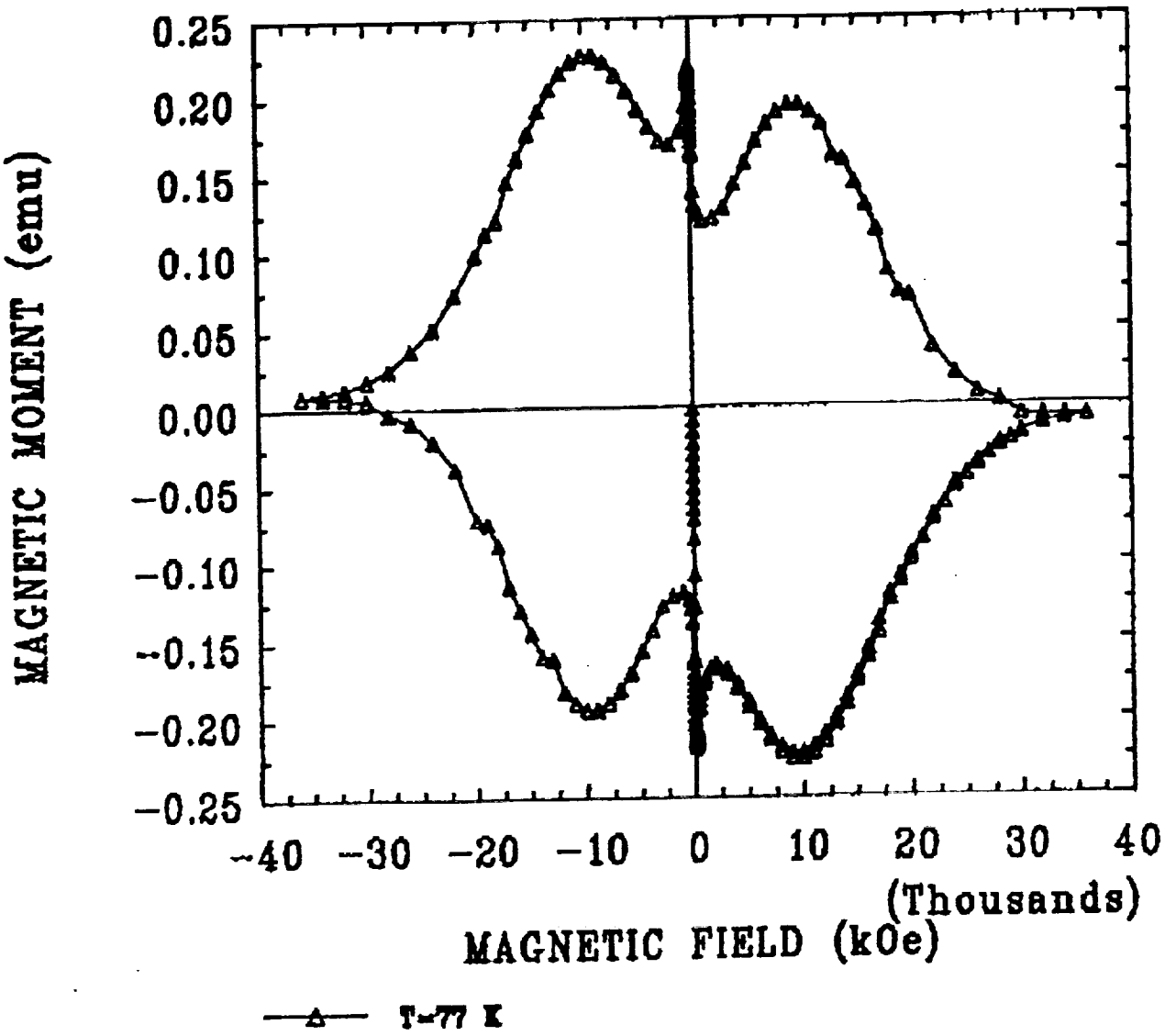


Fig. 7 Full magnetic hysteresis curve at 77 K for the melt processed Pr-Y-Ba-Cu-O sample showing magnetic anomaly.

RD

Fig 7

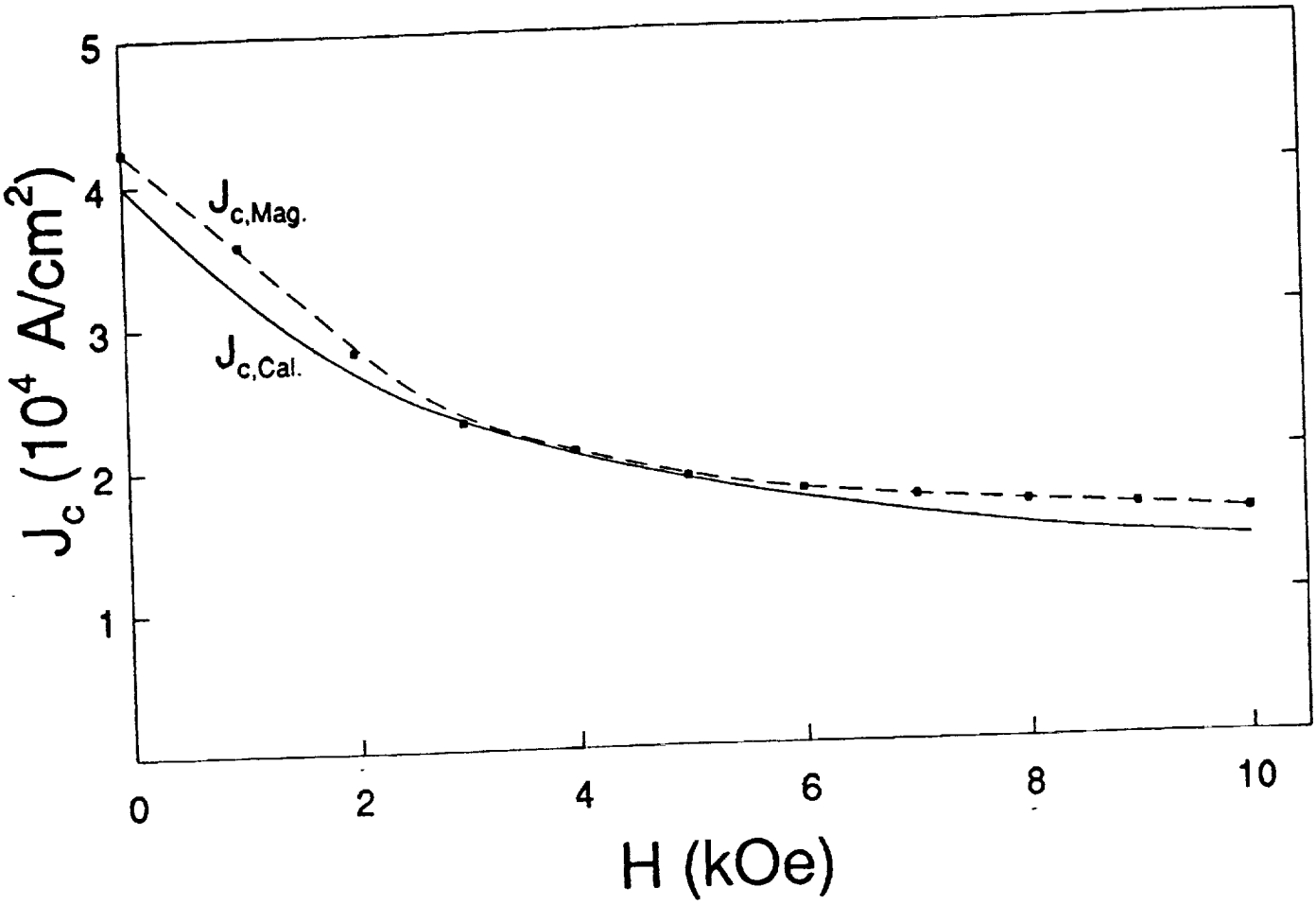


Fig. 8 Critical current density as a function of applied field at 77 K based on the magnetization measurements and the theoretical calculation of Equation 5 for the melt processed Y-Ba-Cu-O sample of Figure 3.

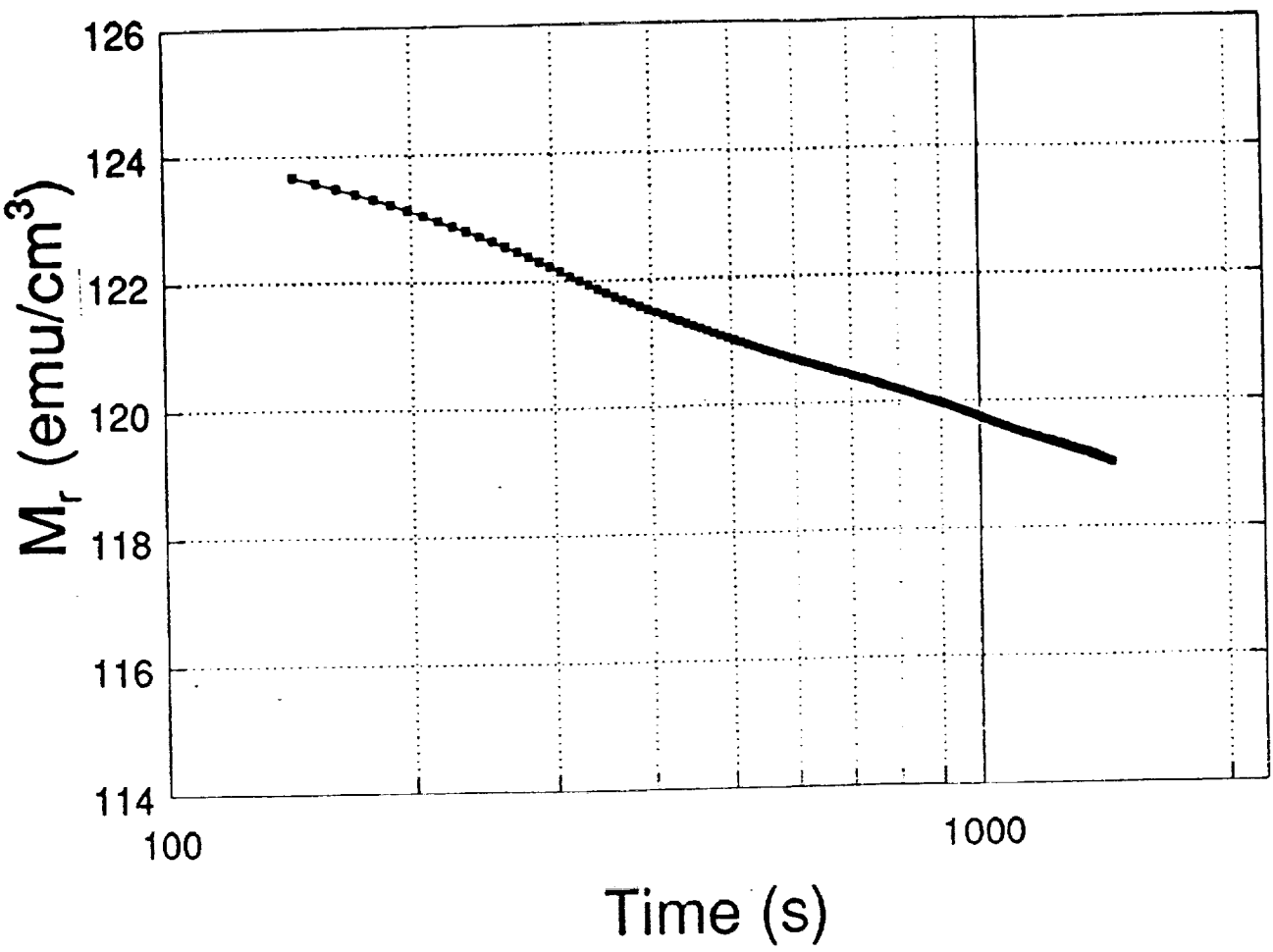


Fig. 9A Decay of the remanent magnetization at 77 K with the charging field of 7.5 kOe being parallel to the c-axis of the melt processed Y-Ba-Cu-O sample of Figures 3 & 8.



Fig 9.A

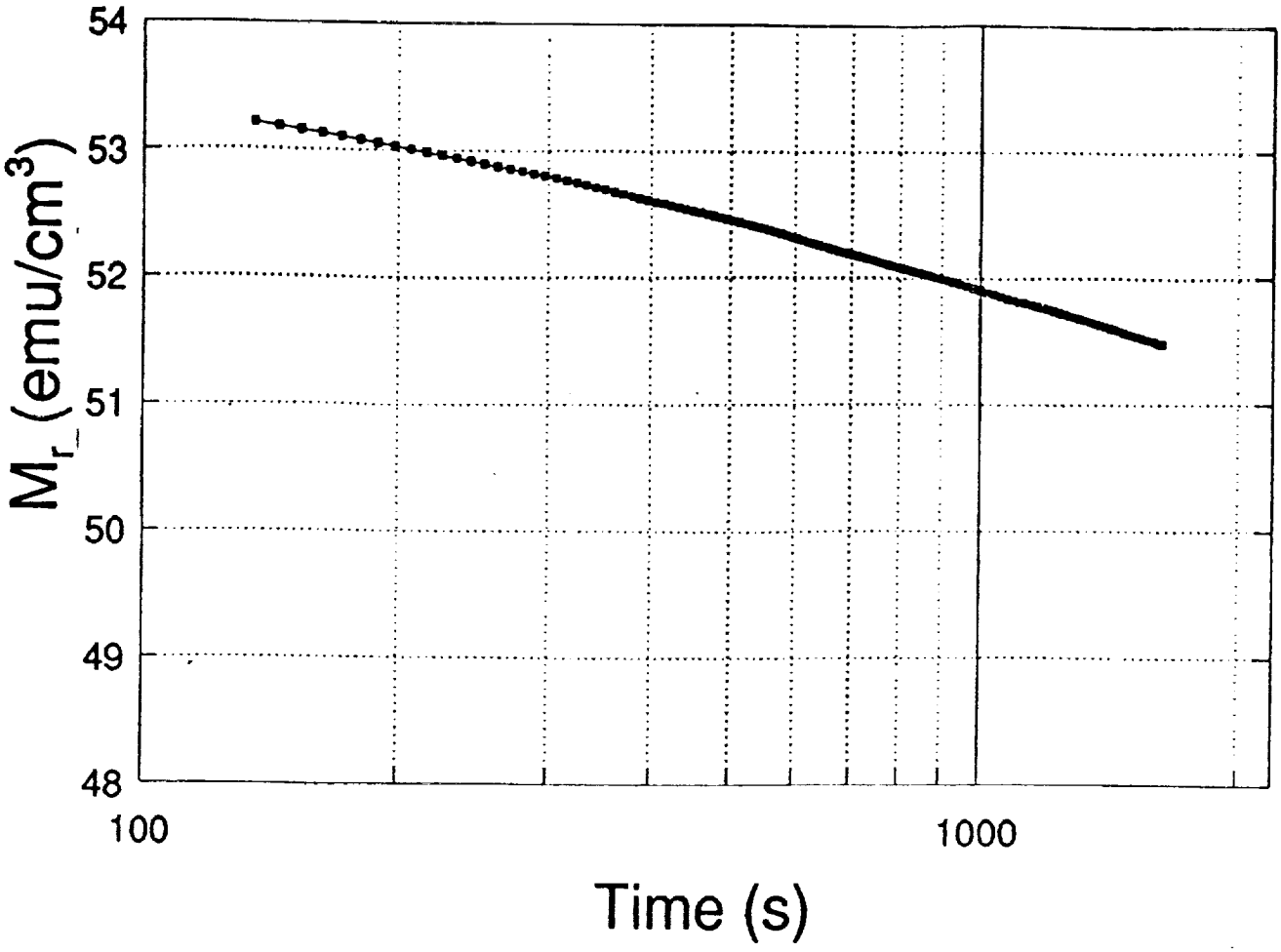


Fig. 9B Decay of the remanent magnetization at 77 K with the charging field of 7.5 kOe being perpendicular to the c-axis of the melt processed Y-Ba-Cu-O sample of Figures 3 & 8.

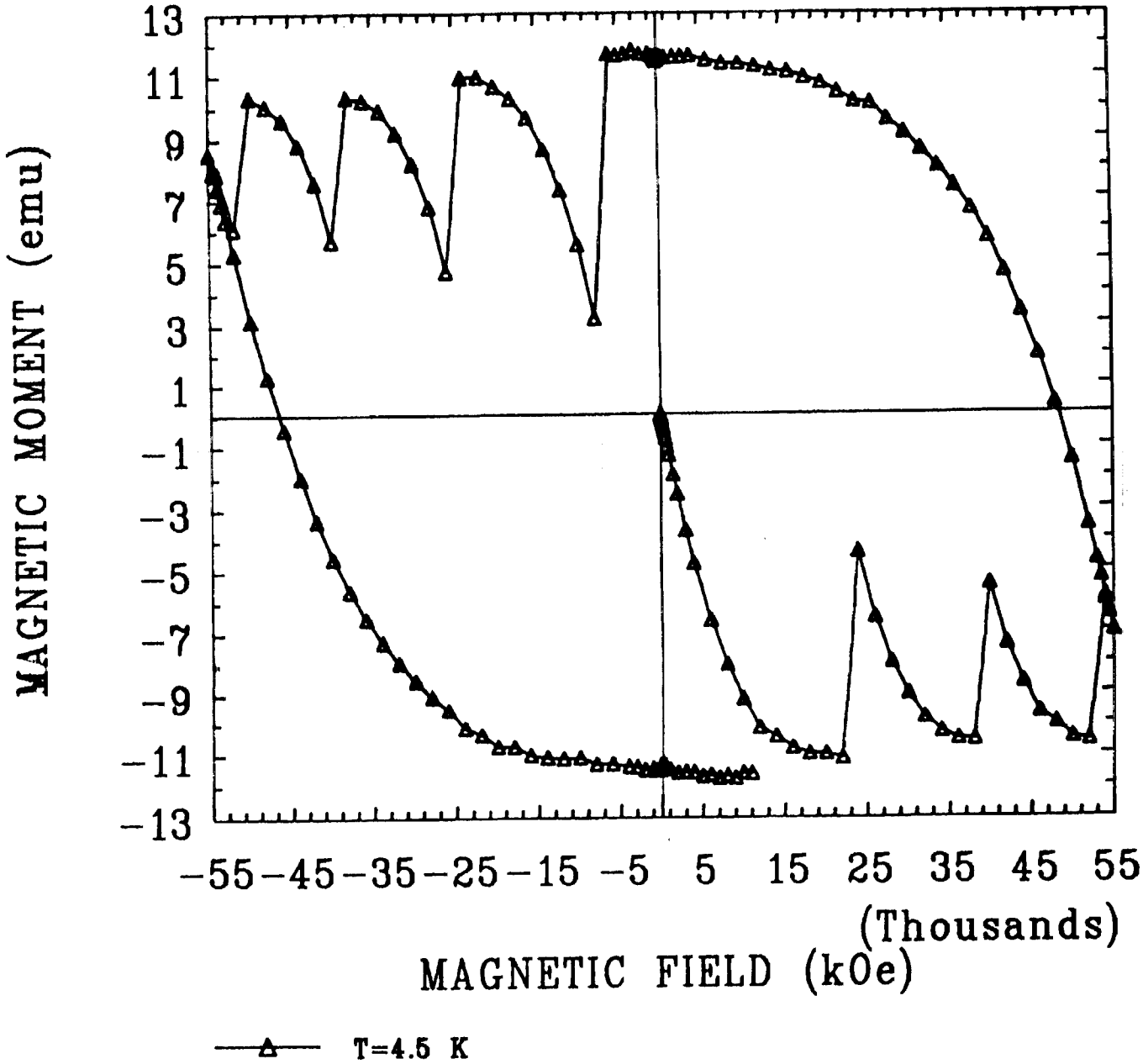


Fig. 10 Magnetic hysteresis curve at 4.5 K for the melt processed Pr-Y-Ba-Cu-O sample of Figures 6 and 7 showing flux jumps.

# Schematic Presentation of Coupling Effect

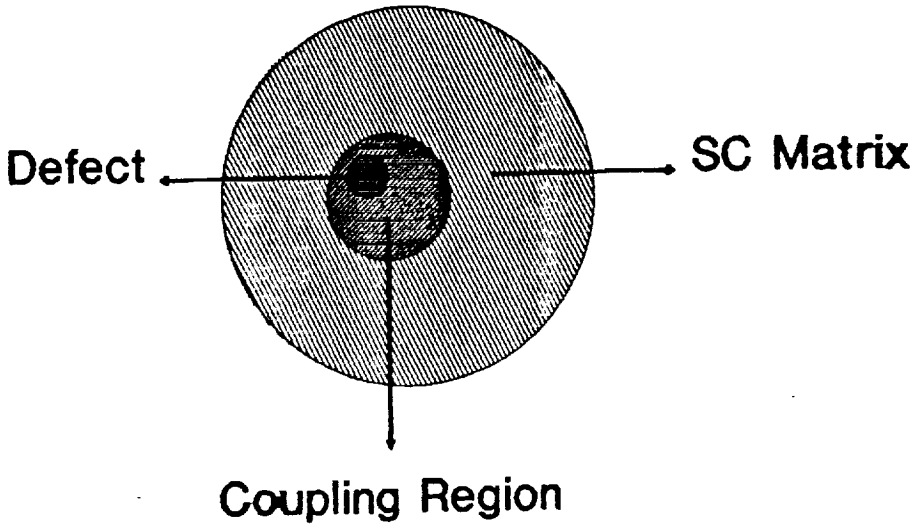


Fig. 11 Schematic presentation of the coupling effect.

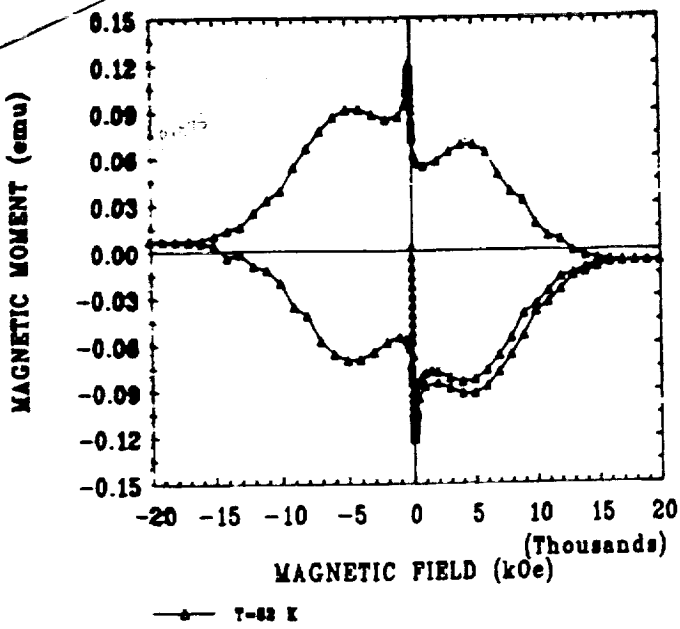
MAGNETIC MOMENT (emu)
0.15
0.12
0.09
0.06
0.03
0.00
-0.03
-0.06
-0.09
-0.12
-0.15
-20 -15 -10 -5 0 5 10 15 20
(Thousands)
MAGNETIC FIELD (kOe)
T=82 K

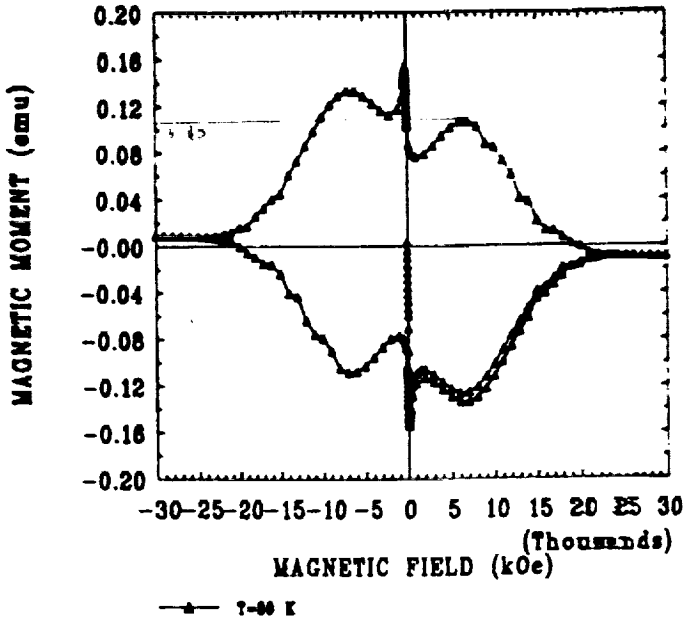
MAGNETIC MOMENT (emu)
0.20
0.16
0.12
0.08
0.04
0.00
-0.04
-0.08
-0.12
-0.16
-0.20
-30-25-20-15-10-5 0 5 10 15 20 25 30
(Thousands)
MAGNETIC FIELD (kOe)
T=80 K

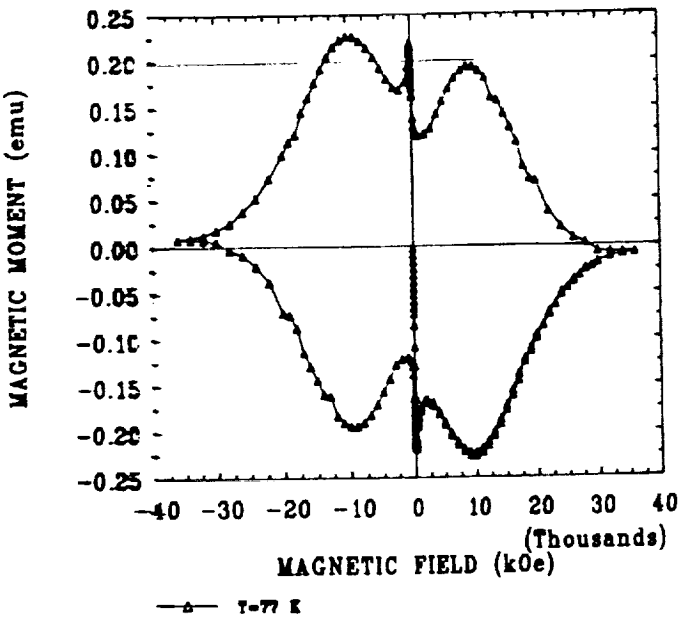
MAGNETIC MOMENT (emu)
0.25
0.20
0.15
0.10
0.05
0.00
-0.05
-0.10
-0.15
-0.20
-0.25
-40 -30 -20 -10 0 10 20 30 40
(Thousands)
MAGNETIC FIELD (kOe)
T=77 K

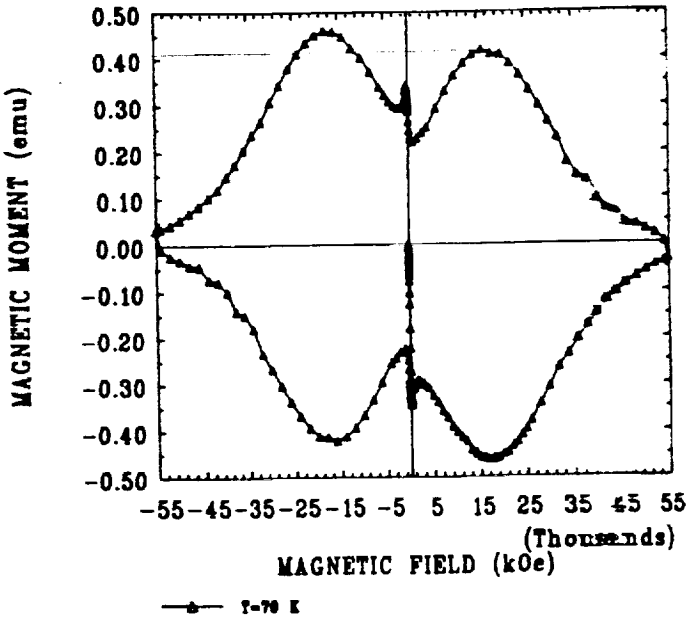
MAGNETIC MOMENT (emu)
0.50
0.40
0.30
0.20
0.10
0.00
-0.10
-0.20
-0.30
-0.40
-0.50
-55-45-35-25-15 -5 5 15 25 35 45 55
(Thousands)
MAGNETIC FIELD (kOe)
T=70 K

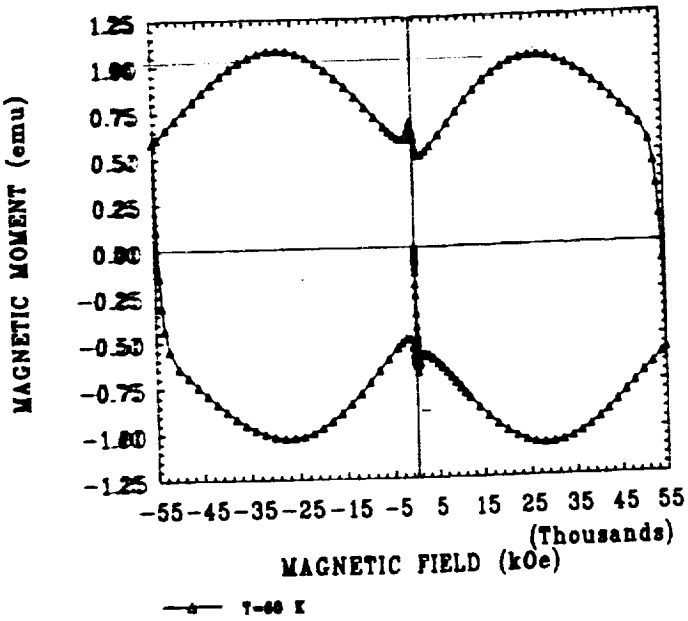
MAGNETIC MOMENT (emu)
1.25
0.75
-0.75
-1.25
-55-45-35-25-15 -5 5 15 25 35 45 55
(Thousands)
MAGNETIC FIELD (kOe)
T=60 K

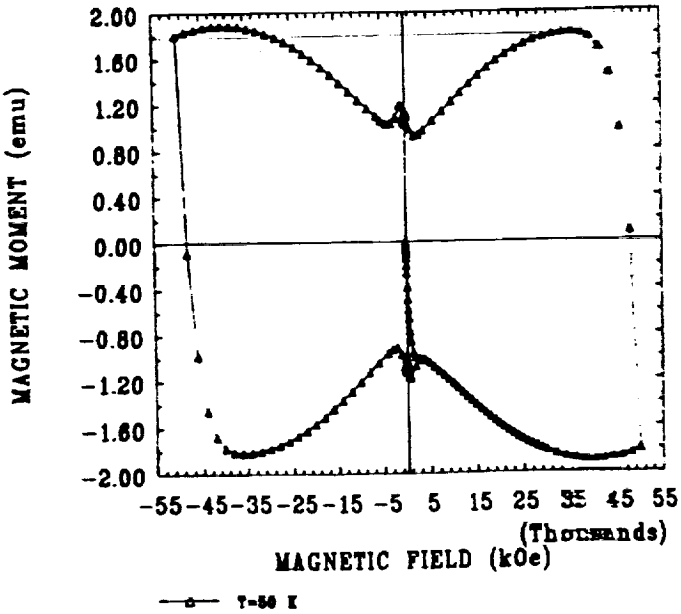
MAGNETIC MOMENT (emu)
2.00
1.60
1.20
0.80
0.40
0.00
-0.40
-0.80
-1.20
-1.60
-2.00
-55-45-35-25-15 -5 5 15 25 35 45 55
(Thousands)
MAGNETIC FIELD (kOe)
T=50 K

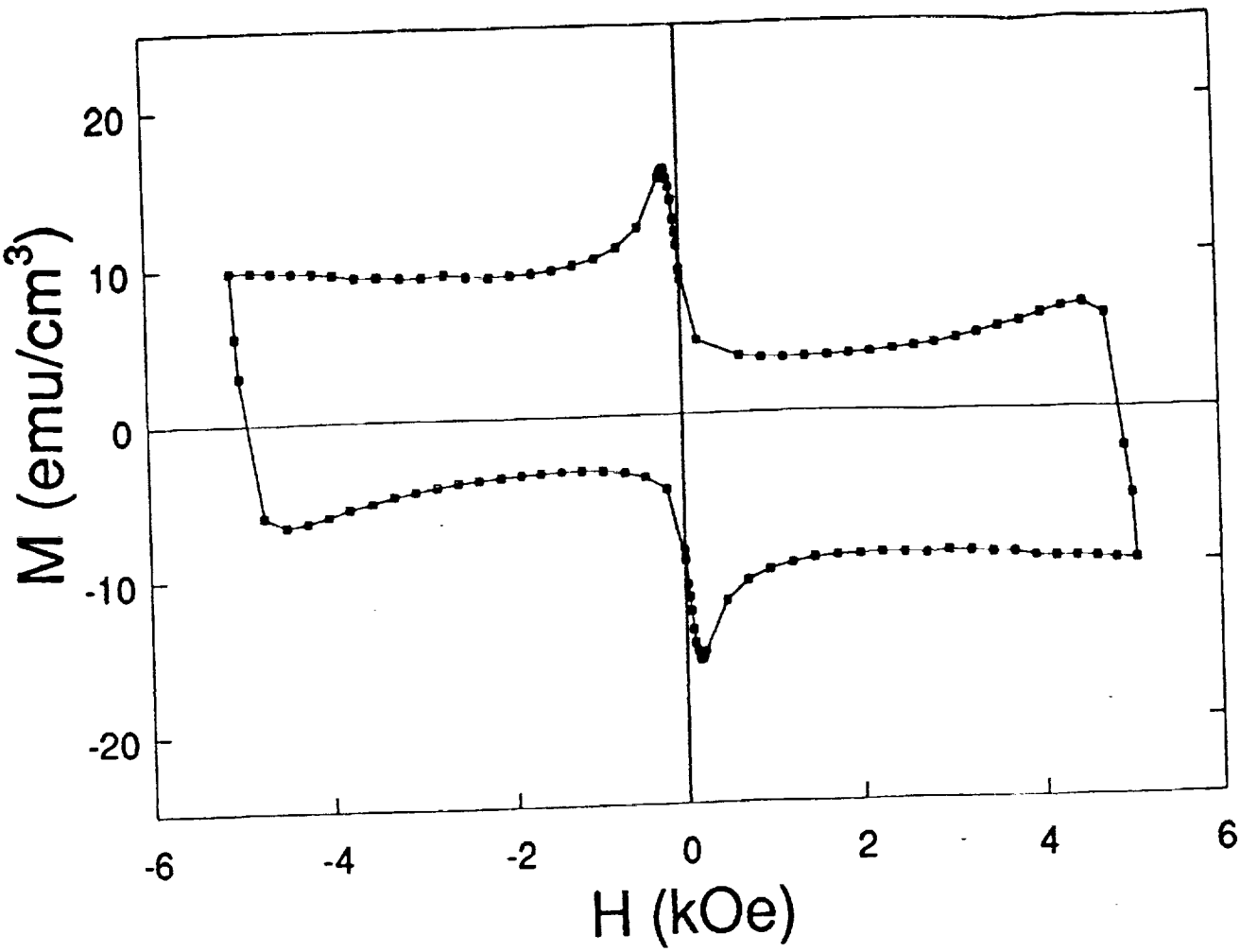


Fig. 13 Magnetic hysteresis curve at 77 K for a melt processed Bi-Y-Ba-Cu-O sample.



Fig 13

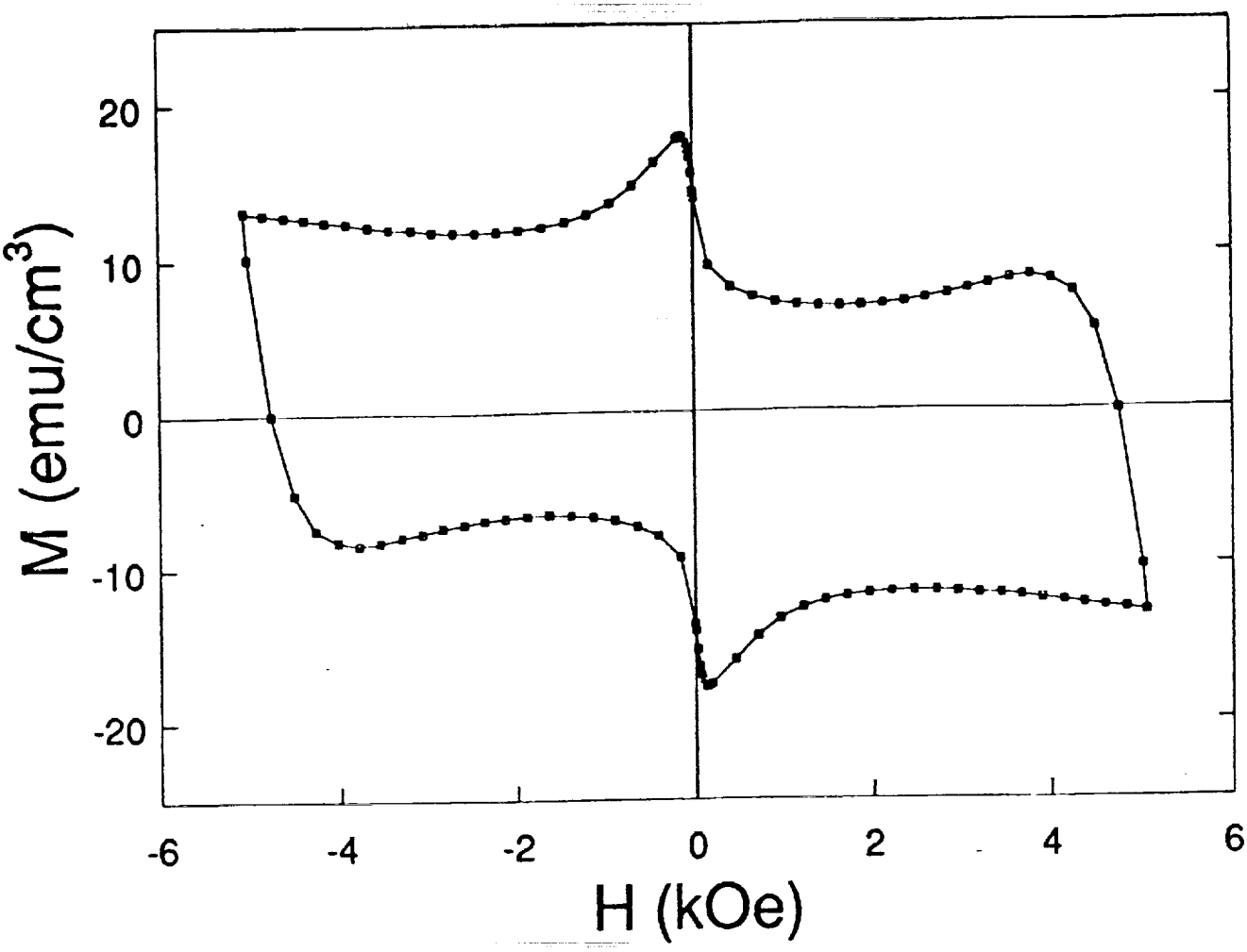


Fig. 14 Magnetic hysteresis curve at 77 K for a melt processed In-Y-Ba-Cu-O sample.

Fig 14